

Controlled-phase gate for photons based on stationary light

Ivan Iakoupov¹, Johannes Borregaard^{1,2}, and Anders S. Sørensen¹

¹ *The Niels Bohr Institute, University of Copenhagen, Blegdamsvej 17, DK-2100 Copenhagen Ø, Denmark*

² *Department of Physics, Harvard University, Cambridge, MA 02138, USA*

(Dated: January 8, 2018)

We propose a method to induce strong effective interactions between photons mediated by an atomic ensemble. To achieve this, we use the so-called stationary light effect to enhance the interaction. Regardless of the single-atom coupling to light, the interaction strength between the photons can be enhanced by increasing the total number of atoms. For sufficiently many atoms, the setup can be viable as a controlled-phase gate for photons. We derive analytical expressions for the fidelities for two modes of gate operation: deterministic and heralded conditioned on the presence of two photons at the output.

Optical photons are ideal carriers of quantum information over long distances, and such quantum communication may enable a wealth of applications [1]. Quantum information processing with photonic qubits is, however, severely limited by the lack of efficient two-qubit gates. In principle, such gates could be realized by strongly coupling photons to a single atom [2, 3]. Experiments have pushed towards realizing such strong coupling, e.g. in cavity QED structures [4–8] and optical waveguides [9–12], but the realization of two-qubit gates remains challenging. For some applications, it is possible to use atomic ensembles where a large number of atoms compensates for a weak single-atom coupling strength [13]. However, this approach typically does not enhance the nonlinear interactions required for quantum gates. Gate operation is often pursued by extending the ensemble approach with strong dipole-dipole interactions of the atomic Rydberg levels [14–19]. In recent years, experiments in e.g. tapered optical fibers [20–24] and hollow core photonic-crystal fibers [25, 26] have realized an intermediate regime where the single-atom coupling to light is sizeable, but still not sufficient to realize photonic gates based on single atoms. It remains an open question to which degree such moderate couplings enable processing of quantum information.

In this letter, we propose a controlled-phase gate that works even if the individual atoms are not coupled strongly either to light (e.g. optical cavities) or to each other (e.g. Rydberg interactions). We show that by using sufficiently many atoms, it is possible to compensate for the limited single-atom coupling to light and achieve ideal gate operation [27]. The main physical mechanism behind the gate is *stationary light* [28, 29] where polaritons (coupled light-matter excitations) have very low group velocity due to counter-propagating classical drives. These polaritons experience reflections at the ends of the ensemble. This leads to transmission resonances whenever the polaritons form standing waves inside the ensemble [27], akin to an optical cavity. We show that the storage of a single photon completely changes the scattering properties of the ensemble because the

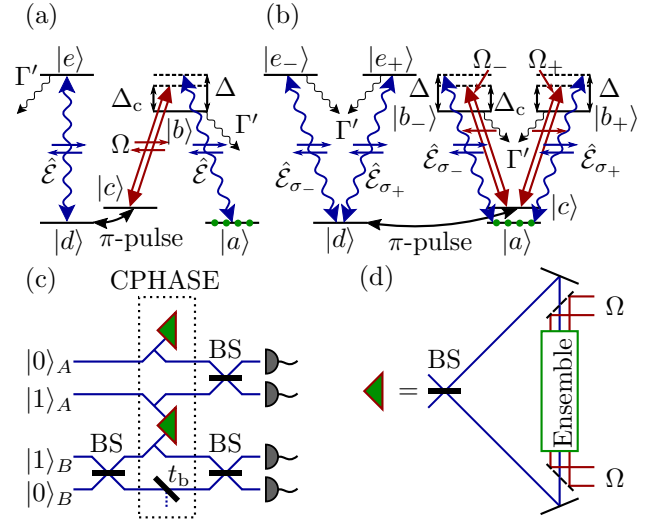


FIG. 1. (Color online) (a) Level diagram of Λ -type atoms (levels $|a\rangle$, $|b\rangle$, and $|c\rangle$) that can be switched to two-level atoms (levels $|d\rangle$ and $|e\rangle$) by the storage of a photon followed by a π -pulse. Green dots indicate the initial state of the atoms. (b) Level diagram of dual-V atoms that can be switched to V-type atoms. (c) Dual-rail Bell-state measurement setup with the controlled-phase gate (CPHASE) as a part of it. An ensemble of atoms is placed inside a Sagnac interferometer, shown as a triangle in (c) and defined by (d). In the rail corresponding to state $|0\rangle_B$, a beam splitter is added with transmission coefficient t_b . All the other beam splitters (BS) are 50:50.

cavity-like structure created by the remaining atoms enhances the interaction with the stored excitation. This can be used to mediate a gate between photons that can be either deterministic or heralded (successful operation is conditioned on subsequent detection of two photons).

Overview. We consider two different level schemes for the atoms in the ensemble: Λ -type and dual-V (Figs. 1(a) and 1(b), respectively). The linear properties of these two schemes are described in detail in Ref. [30]. In the Λ -type scheme, two counter-propagating classical drives have the same polarization and frequency.

This results in a standing wave of the Rabi frequency $\Omega(z) = \Omega_0 \cos(k_0 z)$, where k_0 is the wave vector of the classical drive, assumed to be the same as the wave vector of the probe field $\hat{\mathcal{E}}$ (single photon). For the Λ -type scheme, we assume that N atoms are placed at positions $z_j = j\pi/(2k_0)$ with $0 \leq j \leq N-1$ to achieve the lowest possible group velocity (increasing the interatomic distance by integer multiples of π/k_0 does not change the results) [30]. Low group velocity can also be achieved by separating the two counter-propagating classical drives either in polarization [31] or frequency [32]. We choose the separation in polarization, i.e. the dual-V scheme, but separation in frequency is expected to yield similar results [30]. From a practical perspective, the dual-V scheme is desirable since it does not require careful placement of the atoms. However, we focus on the Λ -type scheme in the analysis below, since it admits an approximate analytical solution. We also perform the numerical analysis for both of the schemes and show that the analytical results obtained for the Λ -type scheme provide the correct scaling for the dual-V scheme.

The single-atom coupling to light is characterized by the parameter Γ_{1D}/Γ (half of the resonant optical depth per atom), where Γ_{1D} is the decay rate from each of the states $|b\rangle$ and $|e\rangle$ (see Fig. 1(a)) into both right-moving and left-moving guided modes (assumed to be equal), Γ' is the decay rate into all the other modes, and $\Gamma = \Gamma_{1D} + \Gamma'$ is the total decay rate. In the dual-rail encoding of photonic qubits shown in Fig. 1(c), two identical atomic ensembles are required, where the upper one only functions as a memory. Alternatively, the single-rail encoding can also be implemented with one atomic ensemble [18], but the dual-rail encoding allows heralded operation that has better fidelity. Each ensemble is placed inside a Sagnac interferometer (Fig. 1(d)).

The operation of the CP gate is sequential. First, photon A is stored either in the upper ($|0\rangle_A$) or the lower ($|1\rangle_A$) ensemble using electromagnetically induced transparency (EIT) [33]. Then photon B is scattered from the lower ensemble under stationary light conditions ($|1\rangle_B$) or passes through a beam splitter with transmission coefficient t_b ($|0\rangle_B$). The role of this beam splitter will be explained below. The Sagnac interferometer can be set up such that most of the incident power in each of its two input ports is reflected back through the same port, regardless of whether the ensemble is reflective or transmissive [34, 35]. Reflection or transmission of the ensemble instead controls the phase of the reflected field. The scattering of photon B can be arranged such that if there is no stored photon in the lower ensemble (photon A is in the state $|0\rangle_A$), the atomic ensemble is completely transmissive in the ideal case, and photon B is reflected from the Sagnac interferometer with no additional phase. If there is a stored photon (photon A is in state $|1\rangle_A$), photon B is reflected from the interferometer with a π phase shift. The latter case performs the desired controlled-

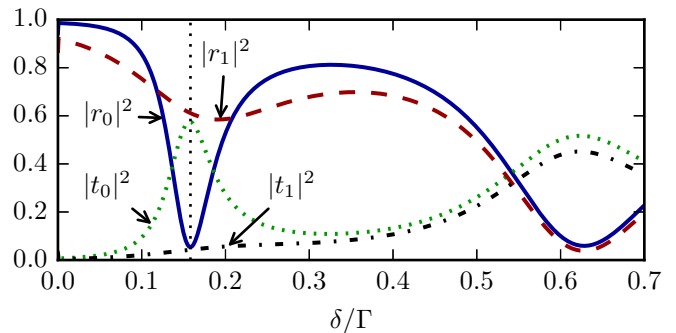


FIG. 2. (Color online) (a) Reflectances ($|r_0|^2$, $|r_1|^2$) and transmittances ($|t_0|^2$, $|t_1|^2$) of an ensemble of Λ -type atoms without ($|r_0|^2$, $|t_0|^2$) and with ($|r_1|^2$, $|t_1|^2$) a stored photon for different frequencies (two-photon detunings) δ . The vertical dotted line marks the operation point δ_{res} . The parameters are: $N = 10^4$, $\Gamma_{1D}/\Gamma = 0.05$, $\Delta_c/\Gamma = -10$, and $\Omega_0/\Gamma = 10$.

phase gate operation $|11\rangle_{AB} \rightarrow -|11\rangle_{AB}$, while the rest of the basis states are unchanged. Finally, photon A is retrieved using EIT.

Storage and retrieval. Before the EIT storage, all atoms are initialized in state $|a\rangle$, and after storage, the incident photon is mapped onto an atom being in state $|c\rangle$. To produce an optical non-linearity, we assume that state $|c\rangle$ is subsequently transferred to state $|d\rangle$ using a π -pulse. Under EIT storage and retrieval, both the incident photon and the classical drive are assumed resonant with the respective atomic transitions for simplicity. The classical drive is incident from one side only. Entering the Sagnac interferometer, photon A is split into two parts by the 50:50 beam splitter (see Fig. 1(d)). The two parts reach the ensemble from the opposite sides with opposite spatial phase factors $e^{ik_0 z}$ and $e^{-ik_0 z}$. Inside the ensemble, the two parts will interfere, resulting in a stored spin wave with $\cos(k_0 z)$ spatial modulation. Such storage procedure is necessary (for the Λ -type scheme only), since the part of the excitation that is stored on the nodes of the standing wave of the classical drive (that is applied during scattering of photon B) does not change the scattering properties of the ensemble.

Reflection and transmission. We use the (multi-mode) transfer matrix formalism [30, 36] to model the scattering process. To illustrate the scattering behavior, we assume that photon A was stored in the center of the atomic ensemble at an anti-node of the classical drive. The reflectances and transmittances of an ensemble of Λ -type atoms are plotted in Fig. 2 as functions of the two-photon detuning $\delta = \Delta - \Delta_c$, where Δ (Δ_c) is the detuning of the probe field (classical drive). The reflectance $|r_0|^2$ ($|r_1|^2$) and transmittance $|t_0|^2$ ($|t_1|^2$) are for an ensemble without (with) a stored photon. The ensemble is seen to have transmittance resonances with a large $|t_0|^2$ and a small $|r_0|^2$. These resonances occur when the standing wave

condition is fulfilled, i.e. $\sin(qL) = 0$, where q is the Bloch vector of the stationary light polaritons and L is the length of the ensemble [27, 30]. When a photon is stored in the ensemble, an atom changes from state $|a\rangle$ to $|d\rangle$. In state $|d\rangle$, the atom acts as a two-level atom that is resonant with the incident photon (see Fig. 1(a)). Since the effective interaction is enhanced by the cavity-like behavior of the ensemble, this single two-level atom can make the entire ensemble become reflective instead of transmissive.

We focus on the behavior at the resonance nearest $\delta = 0$ (vertical dotted line in Fig. 2). In the limit of large atom number N and for $|\Delta_c| \neq 0$, this resonance is at a two-photon detuning $\delta_{\text{res}} \approx -4\pi^2\Delta_c|\Omega_0|^2/(\Gamma_{1D}^2N^2)$ for which we obtain [37]

$$r_0 \approx \frac{\Gamma_{1D}\Gamma'N}{16\Delta_c^2}, \quad (1)$$

$$t_0 \approx 1 - r_0, \quad (2)$$

$$r_1(\tilde{z}) \approx 1 - \frac{4\pi^2\Delta_c^2\Gamma'}{\Gamma_{1D}^3N^2} - \frac{4i\pi^2\Delta_c}{\Gamma_{1D}N} \left(\tilde{z} - \frac{1}{2} \right) - \frac{4\pi^4\Delta_c^2(2\Gamma_{1D} + \Gamma')}{\Gamma_{1D}^3N^2} \left(\tilde{z} - \frac{1}{2} \right)^2, \quad (3)$$

$$t_1(\tilde{z}) \approx \frac{4\pi^2\Delta_c^2\Gamma'}{\Gamma_{1D}^3N^2} + \frac{8\pi^4\Delta_c^2\Gamma'}{\Gamma_{1D}^3N^3} \left(\tilde{z} - \frac{1}{2} \right) + \frac{4\pi^4\Delta_c^2\Gamma'}{\Gamma_{1D}^3N^2} \left(\tilde{z} - \frac{1}{2} \right)^2. \quad (4)$$

Here, t_1 and r_1 were obtained by solving the discrete problem where a photon is stored in a single discrete atom, and then taking the continuum limit such that the index of the atom is replaced by its position inside the ensemble $\tilde{z} = z/L$. By aligning the interferometer, the reflection coefficients of the combined interferometer-ensemble system are given by $R_0 = -(r_0 - t_0)$ and $R_1(\tilde{z}) = -(r_1(\tilde{z}) - t_1(\tilde{z}))$ [37]. If we take $\tilde{z} = 1/2$ and a detuning $|\Delta_c| \sim \Gamma_{1D}N^{3/4}$, we have $r_0, t_1 \sim \Gamma'/(\Gamma_{1D}\sqrt{N})$, $r_1 \approx 1 - t_1$, and $t_0 \approx 1 - r_0$. Hence, even for small Γ_{1D}/Γ' , we can achieve an ideal CP gate ($R_0 = 1$, $R_1 = -1$) with sufficiently many atoms.

Fidelity. To quantify the errors of the gate, we calculate the Choi-Jamiolkowski (CJ) fidelity [18, 38]. The EIT storage is described using the storage K_s and retrieval K_r kernels derived in Ref. [33] (suitably modified to take into account storage from both directions [37]). When photon A is stored and retrieved without scattering of photon B , the output wave function of photon A is $\phi_{A,\text{out},0}(t) = \iint K_r(\tilde{z}, t)K_s(\tilde{z}, t')\phi_{A,\text{in}}(t') dt' d\tilde{z}$, where $\phi_{A,\text{in}}$ is the input wave function. The efficiency of the storage and retrieval is $\eta_{\text{EIT}} = \int |\phi_{A,\text{out},0}(t)|^2 dt$. If photon B was reflected from the interferometer while photon A was stored in the ensemble (state $|11\rangle_{AB}$), the output wave function is instead $\phi_{A,\text{out},1}(t) = \iint K_r(\tilde{z}, t)R_1(\tilde{z})K_s(\tilde{z}, t')\phi_{A,\text{in}}(t') dt' d\tilde{z}$.

Neglecting bandwidth effects of photon B to find the upper limit set by the atomic ensemble, we obtain the CJ fidelity [38–40]

$$F_{\text{CJ}} = \frac{\eta_{\text{EIT}}}{16} |2t_b + R_0 - R_{1,1}|^2, \quad (5)$$

where $R_{1,1} = (1/\eta_{\text{EIT}}) \int \phi_{A,\text{out},0}^*(t)\phi_{A,\text{out},1}(t) dt$. If the gate is conditioned on the presence of two photons after the gate operation [18, 41, 42], we find the success probability

$$P_{\text{suc}} = \frac{\eta_{\text{EIT}}}{4} \left(2|t_b|^2 + |R_0|^2 + R_{1,2} \right), \quad (6)$$

with $R_{1,2} = (1/\eta_{\text{EIT}}) \int |\phi_{A,\text{out},1}(t)|^2 dt$. The conditional CJ fidelity is $F_{\text{CJ,cond}} = F_{\text{CJ}}/P_{\text{suc}}$.

To optimize the performance of the gate, we set $t_b = 1$ and optimize Δ_c and the width of the stored spin wave $\tilde{\sigma} = \sigma/L$ such that F_{CJ} is maximal. In Fig. 3 we plot the numerically calculated $F_{\text{CJ}} \approx P_{\text{suc}}$ and $F_{\text{CJ,cond}}$, where photon A was chosen to have a Gaussian temporal profile, and photon B is centered on $\delta = \delta_{\text{res}}$ and assumed to be narrow in frequency compared to the resonance width. As seen in the figure, both F_{CJ} and $F_{\text{CJ,cond}}$ approach their ideal value of unity for large N , but $F_{\text{CJ,cond}}$ approaches it much faster.

For large N , we can find analytical expressions for the Λ -type curves in Fig. 3 if we neglect distortions of photon A under storage and retrieval, but still account for the errors due to the spatial extent of the stored excitation. The stored spin wave is approximately Gaussian of the form $S(\tilde{z}) = (2\pi\tilde{\sigma}^2)^{-1/4} \exp(-(\tilde{z} - 1/2)^2/(4\tilde{\sigma}^2))$. Consequently, $\eta_{\text{EIT}} \approx 1 - \Gamma'/(2N\Gamma_{1D}\tilde{\sigma}^2)$ [37, 43], $R_{1,1} \approx \int R_{1,s}(\tilde{z})|S(\tilde{z})|^2 d\tilde{z}$, and $R_{1,2} \approx \int |R_{1,s}(\tilde{z})|^2|S(\tilde{z})|^2 d\tilde{z}$. Here, $R_{1,s}(\tilde{z}) = (R_1(\tilde{z}) + R_1(1 - \tilde{z}))/2$ is the symmetrized version of R_1 that accounts for storage and scattering from both sides of the ensemble.

For fixed Γ_{1D} and large N , after choosing $\tilde{\sigma}^2 = 1/(\pi^{3/2}N^{1/4})\sqrt{\Gamma'}/(\Gamma_{1D} + \Gamma')$, $\Delta_c^2 = (\Gamma_{1D}^2N^{3/2})/(8\pi)$, and $t_b = 1$, F_{CJ} is maximal, and

$$F_{\text{CJ},t_b=1} \approx P_{\text{suc},t_b=1} \approx 1 - \frac{\pi\Gamma'}{\Gamma_{1D}\sqrt{N}}, \quad (7)$$

$$F_{\text{CJ,cond},t_b=1} \approx 1 - \frac{\pi^2\Gamma'^2}{4\Gamma_{1D}^2N}. \quad (8)$$

These expressions confirm that the gate fidelity improves with N and that the conditional fidelity has better scaling.

With $t_b = 1$, the losses are different for the different computational basis states. By setting $t_b \approx R_0$ we approximately equalize the losses, leading to a substantial improvement of $F_{\text{CJ,cond}}$ at the cost of increasing $1 - P_{\text{suc}}$ by a constant factor. Whether this is a desirable trade off, depends on the particular application. Taking the

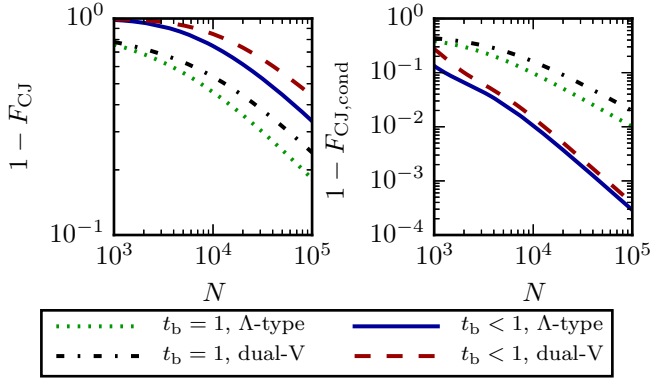


FIG. 3. (Color online) Numerically calculated F_{CJ} and $F_{CJ,cond}$. For the $t_b < 1$ curves, t_b is optimized numerically such that $F_{CJ,cond}$ is maximal. The dual-V scheme uses regular interatomic distance $d = 0.266\pi/k_0$. The common parameters are $\Gamma_{1D}/\Gamma = 0.05$, and $\Omega_0/\Gamma = 1$. Under EIT (storage and retrieval), $\Omega(z) = \Omega_0$. Under stationary light (scattering), $\Omega(z) = \Omega_0 \cos(k_0 z)$ and $\Omega_{\pm}(z) = \Omega_0 e^{\pm i k_0 z}$ for Λ -type and dual-V respectively.

same values of Δ_c and $\tilde{\sigma}$,

$$F_{CJ,t_b=R_0} \approx P_{suc,t_b=R_0} \approx 1 - \frac{2\pi\Gamma'}{\Gamma_{1D}\sqrt{N}}, \quad (9)$$

$$F_{CJ,cond,t_b=R_0} \approx 1 - \frac{11\pi^3 (\Gamma_{1D} + \Gamma') \Gamma'}{16\Gamma_{1D}^2 N^{3/2}}. \quad (10)$$

Here, $1 - F_{CJ,cond}$ is limited by the non-zero $\tilde{\sigma}$.

Numerical simulations suggest that the fidelities are independent of Ω_0 over a wide range of values. E.g. for $\Gamma_{1D}/\Gamma = 0.05$ and $N = 10^4$, $|\Omega_0|$ up to 30Γ with a negligible change in the optimal Δ_c , and to at least 100Γ with some increase in the optimal Δ_c [37].

Dual-V scheme. First, some technical differences from the Λ -type scheme. The decay rate Γ_{1D} is from each of the states $|b_{\pm}\rangle$ and $|e_{\pm}\rangle$ (see Fig. 1(b)). When switched to state $|d\rangle$, the atom becomes a resonant V-type atom. For storage and retrieval, the Λ -type and dual-V schemes behave the same, since only one classical drive is incident. For the numerical calculation of the fidelities for the dual-V scheme in Fig. 3, the distance d between the atoms was set to be incommensurate with the wavelength of the classical drive, $d = 0.266\pi/k_0$. The results are, however, almost independent of d , and the gate can function even with completely random placement of the atoms [37]. The dual-V scheme is seen to have the same scaling as the Λ -type scheme.

Gate time. The total gate time is split between EIT storage and retrieval, two π -pulses, and scattering. The EIT time t_{EIT} is equal to the time to pass the ensemble, i.e. $t_{EIT} \sim L/v_g$, where $v_g = (2L|\Omega_0|^2)/(N\Gamma_{1D})$ is the EIT group velocity [43]. The π -pulse time t_{π} is set by the splitting between states $|a\rangle$ and $|d\rangle$. In the supplemental material [37], we discuss a specific implementation in

^{87}Rb where that splitting is proportional to Δ_c , resulting in $t_{\pi} \gtrsim 1/|\Delta_c|$.

To discuss scattering time, we need to model a non-zero bandwidth of photon B . The reflection coefficient R_0 (at $\delta = \delta_{res}$) in Eq. (5) should be replaced by $\int R_0(\delta)|\phi_B(\delta)|^2 d\delta$, where ϕ_B is the frequency distribution of photon B . Since r_1 and t_1 vary much slower than r_0 and t_0 around $\delta = \delta_{res}$ (see Fig. 2), we ignore a similar modification to $R_{1,1}$. By expanding, we get $r_0(\delta) \approx r_0(\delta_{res}) + (2/w^2)(\delta - \delta_{res})^2$ with the resonance width $w = (32\sqrt{2}\pi^2\Delta_c^2|\Omega_0|^2)/(\Gamma_{1D}^3 N^3)$. Defining $\sigma_B^2 = \int (\delta - \delta_{res})^2 |\phi_B(\delta)|^2 d\delta$ (spectral width of photon B) and using the optimal $\Delta_c^2 = (\Gamma_{1D}^2 N^{3/2})/(8\pi)$, this gives a modification of the fidelity $F_{CJ,t_b=1,\sigma_B} \approx F_{CJ,t_b=1} - (\Gamma_{1D}^2 N^3 \sigma_B^2)/(16|\Omega_0|^4 \pi^2)$. Requiring the error from non-zero σ_B to be the same as the error in Eq. (7), we find that the scattering time is $1/\sigma_B = (\Gamma_{1D}^{3/2} N^{7/4})/(4\pi^{3/2} \sqrt{\Gamma'} |\Omega_0|^2)$.

For $\Gamma_{1D}/\Gamma = 0.05$, $N = 10^4$, $|\Omega_0|/\Gamma = 10$, we have $t_{EIT} \sim 5/\Gamma$, $t_{\pi} \gtrsim 1/|\Delta_c| = 0.1/\Gamma$, and $1/\sigma_B \sim 52/\Gamma$. Hence, the scattering time is dominant in the total gate time ($\sim 1.6 \mu\text{s}$ for ^{87}Rb [44]). This is short compared to the coherence time expected for cooled and trapped atoms (e.g. few hundreds of microseconds in Ref. [45]).

Other imperfections. Classical drives may couple states $|a\rangle$ and $|d\rangle$ off-resonantly to the excited states. The coupling of the former results in four-wave mixing noise, but this can be suppressed by a careful choice of the energy levels [37, 46]. The coupling of the latter introduces loss of the stored photon with the effective rate $\Gamma_{eff} \sim \Gamma' |\Omega_0|^2 / \Delta_{hfs}^2$ [37, 47], where Δ_{hfs} is the hyperfine splitting of the ground states ($|a\rangle$ and $|c\rangle$). Hence, the total reduction in success probability during scattering is $\Gamma_{eff}/\sigma_B \sim (\Gamma_{1D}^{3/2} \sqrt{\Gamma'} N^{7/4})/(4\pi^{3/2} \Delta_{hfs}^2)$. E.g. in ^{87}Rb , $\Delta_{hfs}/\Gamma \sim 10^3$ [44], and this error is negligible compared to other losses for $\Gamma_{1D}/\Gamma = 0.05$ and $N = 10^4$ but becomes significant for $N \sim 10^5$.

If the path lengths of the Sagnac interferometer are not completely stabilized, there is an additional error $\sim (k_0 l)^2$, where l is the deviation of the propagation length from the beam splitter to either end of the ensembles due to misalignment [37]. Finally, the heralded gate is rather insensitive to imperfections in the π -pulses. The conditional fidelity will only be affected by the part of the excitation that still remains in states $|c\rangle$ after both π -pulses and is subsequently read out with a wrong phase. This error thus only enters to a higher order and can be eliminated completely by doing EIT retrieval before the second π -pulse [37].

Conclusion. We have shown, how stationary light can be used to create a CP gate between photons. Most importantly, the gate uses a large number of atoms N to compensate for a limited single-atom coupling to light. In particular, the gate can have a rapid convergence as $N^{-3/2}$ towards unit fidelity if it is operated in a heralded

fashion. The gate is ideally suited for the setups currently under development [21–26], where there is a moderate coupling efficiency to light $\Gamma_{1D}/\Gamma \sim 10^{-3} - 10^{-1}$ and total number of atoms $N \sim 10^3 - 10^5$. In the supplemental material [37], we describe how the gate can be directly employed to improve the communication rate of quantum repeaters based on atomic ensembles. In general, the gate may serve as a tool for photonics based quantum information processing.

The research leading to these results was funded by the European Union Seventh Framework Programme through SIQS (Grant No. 600645) and ERC Grant QIOS (Grant No. 306576). J.B. acknowledges funding from the Carlsberg foundation.

Note added. Recently, we became aware of a related study [48].

-
- [1] H. J. Kimble, *Nature* **453**, 1023 (2008).
- [2] L.-M. Duan and H. J. Kimble, *Phys. Rev. Lett.* **92**, 127902 (2004).
- [3] D. E. Chang, A. S. Sørensen, E. A. Demler, and M. D. Lukin, *Nat Phys* **3**, 807 (2007).
- [4] H. Kim, R. Bose, T. C. Shen, G. S. Solomon, and E. Waks, *Nat Photon* **7**, 373 (2013).
- [5] W. Chen, K. M. Beck, R. Bücker, M. Gullans, M. D. Lukin, H. Tanji-Suzuki, and V. Vuletić, *Science* **341**, 768 (2013).
- [6] T. G. Tiecke, J. D. Thompson, N. P. de Leon, L. R. Liu, V. Vuletić, and M. D. Lukin, *Nature* **508**, 241 (2014).
- [7] B. Hacker, S. Welte, G. Rempe, and S. Ritter, *Nature* **536**, 193 (2016).
- [8] J. Volz, M. Scheucher, C. Junge, and A. Rauschenbeutel, *Nat Photon* **8**, 965 (2014).
- [9] A. V. Akimov, A. Mukherjee, C. L. Yu, D. E. Chang, A. S. Zibrov, P. R. Hemmer, H. Park, and M. D. Lukin, *Nature* **450**, 402 (2007).
- [10] J. Claudon, J. Bleuse, N. S. Malik, M. Bazin, P. Jaffrennou, N. Gregersen, C. Sauvan, P. Lalanne, and J.-M. Gérard, *Nat Photon* **4**, 174 (2010).
- [11] A. Goban, C.-L. Hung, S.-P. Yu, J. D. Hood, J. A. Muniz, J. H. Lee, M. J. Martin, A. C. McClung, K. S. Choi, D. E. Chang, O. Painter, and H. J. Kimble, *Nat Commun* **5**, 3808 (2014).
- [12] I. Söllner, S. Mahmoodian, S. L. Hansen, L. Midolo, A. Javadi, G. Kiršanskė, T. Pregolato, H. El-Ella, E. H. Lee, J. D. Song, S. Stobbe, and P. Lodahl, *Nat Nano* **10**, 775 (2015).
- [13] K. Hammerer, A. S. Sørensen, and E. S. Polzik, *Rev. Mod. Phys.* **82**, 1041 (2010).
- [14] M. Saffman, T. G. Walker, and K. Mølmer, *Rev. Mod. Phys.* **82**, 2313 (2010).
- [15] D. Roy, C. M. Wilson, and O. Firstenberg, *Rev. Mod. Phys.* **89**, 021001 (2017).
- [16] A. V. Gorshkov, J. Otterbach, M. Fleischhauer, T. Pohl, and M. D. Lukin, *Phys. Rev. Lett.* **107**, 133602 (2011).
- [17] M. Khazali, K. Heshami, and C. Simon, *Phys. Rev. A* **91**, 030301 (2015).
- [18] S. Das, A. Grankin, I. Iakoupov, E. Brion, J. Borregaard, R. Boddeda, I. Usmani, A. Ourjoumtsev, P. Grangier, and A. S. Sørensen, *Phys. Rev. A* **93**, 040303 (2016).
- [19] C. R. Murray and T. Pohl, *Phys. Rev. X* **7**, 031007 (2017).
- [20] F. Le Kien, V. I. Balykin, and K. Hakuta, *Phys. Rev. A* **70**, 063403 (2004).
- [21] E. Vetsch, D. Reitz, G. Sagué, R. Schmidt, S. T. Dawkins, and A. Rauschenbeutel, *Phys. Rev. Lett.* **104**, 203603 (2010).
- [22] A. Goban, K. S. Choi, D. J. Alton, D. Ding, C. Lacroûte, M. Pototschnig, T. Thiele, N. P. Stern, and H. J. Kimble, *Phys. Rev. Lett.* **109**, 033603 (2012).
- [23] J.-B. Béguin, E. M. Bookjans, S. L. Christensen, H. L. Sørensen, J. H. Müller, E. S. Polzik, and J. Appel, *Phys. Rev. Lett.* **113**, 263603 (2014).
- [24] B. Gouraud, D. Maxein, A. Nicolas, O. Morin, and J. Laurat, *Phys. Rev. Lett.* **114**, 180503 (2015).
- [25] M. Bajcsy, S. Hofferberth, V. Balic, T. Peyronel, M. Hafezi, A. S. Zibrov, V. Vuletic, and M. D. Lukin, *Phys. Rev. Lett.* **102**, 203902 (2009).
- [26] F. Blatt, L. S. Simeonov, T. Halfmann, and T. Peters, *Phys. Rev. A* **94**, 043833 (2016).
- [27] M. Hafezi, D. E. Chang, V. Gritsev, E. Demler, and M. D. Lukin, *Phys. Rev. A* **85**, 013822 (2012).
- [28] A. André and M. D. Lukin, *Phys. Rev. Lett.* **89**, 143602 (2002).
- [29] M. Bajcsy, A. S. Zibrov, and M. D. Lukin, *Nature* **426**, 638 (2003).
- [30] I. Iakoupov, J. R. Ott, D. E. Chang, and A. S. Sørensen, *Phys. Rev. A* **94**, 053824 (2016).
- [31] F. E. Zimmer, J. Otterbach, R. G. Unanyan, B. W. Shore, and M. Fleischhauer, *Phys. Rev. A* **77**, 063823 (2008).
- [32] S. A. Moiseev and B. S. Ham, *Phys. Rev. A* **73**, 033812 (2006).
- [33] A. V. Gorshkov, A. André, M. D. Lukin, and A. S. Sørensen, *Phys. Rev. A* **76**, 033805 (2007).
- [34] G. Bertocchi, O. Alibart, D. B. Ostrowsky, S. Tanzilli, and P. Baldi, *Journal of Physics B: Atomic, Molecular and Optical Physics* **39**, 10 (2006).
- [35] M. Bradford, K. C. Obi, and J.-T. Shen, *Phys. Rev. Lett.* **108**, 103902 (2012).
- [36] I. H. Deutsch, R. J. C. Spreeuw, S. L. Rolston, and W. D. Phillips, *Phys. Rev. A* **52**, 1394 (1995).
- [37] See Supplemental Material for further details. It additionally uses Refs. [49–55].
- [38] A. Gilchrist, N. K. Langford, and M. A. Nielsen, *Phys. Rev. A* **71**, 062310 (2005).
- [39] I. Iakoupov, *Enhancement of optical nonlinearities with stationary light*, Ph.D. thesis, University of Copenhagen (2016).
- [40] I. Iakoupov and A. S. Sørensen, In preparation.
- [41] L.-M. Duan, B. Wang, and H. J. Kimble, *Phys. Rev. A* **72**, 032333 (2005).
- [42] J. Borregaard, P. Kómár, E. M. Kessler, A. S. Sørensen, and M. D. Lukin, *Phys. Rev. Lett.* **114**, 110502 (2015).
- [43] D. E. Chang, A. H. Safavi-Naeini, M. Hafezi, and O. Painter, *New Journal of Physics* **13**, 023003 (2011).
- [44] D. A. Steck, “Rubidium 87 D Line Data,” Available online at <http://steck.us/alkalidata> (revision 2.1.5, 13 January 2015).
- [45] J.-B. Béguin, J. H. Müller, J. Appel, and E. S. Polzik, arXiv:1708.08387.
- [46] P. Walther, M. D. Eisaman, A. André, F. Massou, M. Fleischhauer, A. S. Zibrov, and M. D. Lukin,

- International Journal of Quantum Information **05**, 51 (2007).
- [47] F. Reiter and A. S. Sørensen, Phys. Rev. A **85**, 032111 (2012).
- [48] O. Lahad and O. Firstenberg, Phys. Rev. Lett. **119**, 113601 (2017).
- [49] L.-M. Duan, M. D. Lukin, J. I. Cirac, and P. Zoller, Nature **414**, 413 (2001).
- [50] N. Sangouard, C. Simon, H. de Riedmatten, and N. Gisin, Rev. Mod. Phys. **83**, 33 (2011).
- [51] N. Sangouard, C. Simon, B. Zhao, Y.-A. Chen, H. de Riedmatten, J.-W. Pan, and N. Gisin, Phys. Rev. A **77**, 062301 (2008).
- [52] J. Borregaard, P. Kómár, E. M. Kessler, M. D. Lukin, and A. S. Sørensen, Phys. Rev. A **92**, 012307 (2015).
- [53] T. Peters, Y.-H. Chen, J.-S. Wang, Y.-W. Lin, and I. A. Yu, Opt. Lett. **35**, 151 (2010).
- [54] I. Vurgaftman and M. Bashkansky, Phys. Rev. A **87**, 063836 (2013).
- [55] T. Caneva, M. T. Manzoni, T. Shi, J. S. Douglas, J. I. Cirac, and D. E. Chang, New Journal of Physics **17**, 113001 (2015).

Supplemental Material for “Controlled-phase gate for photons based on stationary light”

CONTENTS

1.	Application to quantum repeaters	7
2.	Implementation in ^{87}Rb atoms	8
3.	Fidelity	10
4.	Scattering coefficients for the ensemble	11
4.1.	Transfer matrix formalism	11
4.2.	Reflection and transmission for the Λ -type scheme	13
4.2.1.	Without a stored photon	13
4.2.2.	With a stored photon	17
4.3.	Reflection and transmission for the dual-V scheme	18
5.	Sagnac interferometer and adjustment of the phases	18
6.	EIT storage and retrieval	20
6.1.	Overview	20
6.2.	Using the dispersion relation	21
6.3.	Using the fully discrete theory	22
6.4.	Using the storage and retrieval kernels	24
7.	Dephasing and decay of the stored photon	28
8.	π -pulses	29
9.	Analytical fidelity of the Λ -type scheme	30
10.	Dependence on positions of the atoms	36
	References	36

1. APPLICATION TO QUANTUM REPEATERS

As a direct application of the proposed CP gate, we consider quantum key distribution using quantum repeaters based on atomic ensembles [S1, S2]. We modify one of the fastest known repeater protocols for atomic ensembles [S3] by implementing the proposed CP gate instead of linear optics for entanglement swapping using the setup in Fig. 1(c) of the main article. The secret key rate per repeater station is calculated as described in Ref. [S4] and compared to the results of the original protocol (see Fig. S4). The secret key rate depends strongly on the repetition rate of the probabilistic single photon sources used at the lowest level of the considered repeater protocol. In the figure, we make the comparison for similar repetition rates as assumed in Ref. [S3]: an optimistic fast rate of 100 MHz and a more realistic of 1 MHz. For completeness, we assume a conservative gate time of 10 μs . The gate time is, however, negligible compared to the time of the single photon generation and the signaling time between stations.

The analysis is similar to the analysis done for the CP gate in Ref. [S5] with the difference that we also consider the possibility of generating the initial entanglement using the CP gate. Generation of initial entanglement is only better than linear optics for very high conditional fidelities of the controlled-phase gate (for $\Gamma_{1D}/\Gamma = 0.5$ and $N \gtrsim 10^3$ in Fig. S4). For low conditional fidelities of the gate, the generation of initial entanglement based on the linear optics as described in Ref. [S3] is better since it essentially has perfect conditional fidelity. For a fair comparison, we consider equal storage and retrieval efficiencies for both protocols. As seen in Fig. S4 for $\Gamma_{1D}/\Gamma = 0.5$, the proposed gate allows improving the rate of quantum repeaters if $N \gtrsim 1000$ for both the considered source repetition rates.

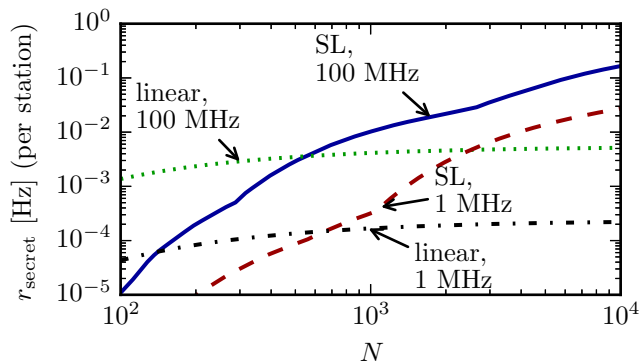


FIG. S4. Secret key rate r_{secret} per repeater station as a function of the number of atoms N with fixed $\Gamma_{1D}/\Gamma = 0.5$ for dual-V atoms with regular interatomic distance $d = 0.266\pi/k_0$. The communication distance is 1000 km. We compare the protocol of Ref. [S3] (“linear”) with a modified protocol where the entanglement swapping (and also initial entanglement generation if it improves r_{secret}) is performed with the proposed stationary light CP gate (“SL”). We consider two different source repetition rates: 100 MHz and 1 MHz. We assume an attenuation length of 22 km in the fibers and an optical signal speed of 2×10^5 km/s. The ensemble storage and retrieval efficiency increases with N and is set to the same value in the original protocol as for the modified one. The photodetector efficiency is assumed to be 90%. The stationary light gate is assumed to have a constant gate time of 10 μs . The steps in the curves occur when the fidelity of the CP gate allows additional swap levels.

2. IMPLEMENTATION IN ^{87}Rb ATOMS

In Fig. S5, we show a possible implementation of the Λ -type scheme (Fig. 1(a) of the main article) on the D_1 line of ^{87}Rb [S6]. The m_F -levels in each manifold are split by the applied magnetic field, so that we can select 3 ground states ($|a\rangle$, $|c\rangle$, and $|d\rangle$) with different energies. The frequency separation between states $|a\rangle$ and $|c\rangle$ is given by the hyperfine splitting Δ_{hfs} . The frequency separations of the other states follow from the requirements

$$\Delta = \omega_0 - \omega_{ab}, \quad (\text{S11})$$

$$0 = \omega_0 - \omega_{de}, \quad (\text{S12})$$

where ω_0 is the carrier frequency of the quantum field, and ω_{ab} and ω_{de} are the atomic transition frequencies. The equations above express the facts that the transition $|a\rangle \leftrightarrow |b\rangle$ has to be off-resonant with detuning Δ , and the transition $|d\rangle \leftrightarrow |e\rangle$ has to be on resonance.

Below, we relate Δ to the required magnetic field strength and determine the splitting between the adjacent m_F -levels in the $F = 2$ manifold that is important for determining the required time for the π -pulse between the levels $|c\rangle$ and $|d\rangle$. The starting point is the expression for the shift in frequency $\Delta_{|F, m_F\rangle}$ of the state $|F, m_F\rangle$ due to a weak magnetic field B_z [S6]

$$\Delta_{|F, m_F\rangle} = \frac{\mu_B}{\hbar} g_F m_F B_z, \quad (\text{S13})$$

where $\mu_B/\hbar = 2\pi \cdot 1.4$ MHz/G is the Bohr magneton in units of the Planck constant, and g_F is the hyperfine Landé g -factor. We follow the convention of using F and m_F for the ground state $5^2S_{1/2}$ and F' and $m_{F'}$ for the excited state $5^2P_{1/2}$. The atomic transition frequencies for the transitions $|a\rangle \leftrightarrow |b\rangle$ and $|d\rangle \leftrightarrow |e\rangle$ can be written

$$\omega_{ab} = \omega_{ab, B_z=0} + \Delta_{|F'=2, m_{F'}=1\rangle} - \Delta_{|F=2, m_F=2\rangle}, \quad (\text{S14})$$

$$\omega_{de} = \omega_{de, B_z=0} + \Delta_{|F'=2, m_{F'}=-2\rangle} - \Delta_{|F=2, m_F=-1\rangle}, \quad (\text{S15})$$

in terms of the transition frequencies $\omega_{ab, B_z=0}$ and $\omega_{de, B_z=0}$ for $B_z = 0$. Note further that $\omega_{ab, B_z=0} = \omega_{de, B_z=0}$, so that we can define $\Delta_a = \omega_0 - \omega_{ab, B_z=0} = \omega_0 - \omega_{de, B_z=0}$. Using this definition together with Eqs. (S13)–(S15) allows to write Eqs. (S11) and (S12)

$$\Delta = \Delta_a - \Delta_{|F'=2, m_{F'}=1\rangle} + \Delta_{|F=2, m_F=2\rangle} = \Delta_a - \frac{\mu_B}{\hbar} g_{F'=2} B_z + 2 \frac{\mu_B}{\hbar} g_{F=2} B_z, \quad (\text{S16})$$

$$0 = \Delta_a - \Delta_{|F'=2, m_{F'}=-2\rangle} + \Delta_{|F=2, m_F=-1\rangle} = \Delta_a + 2 \frac{\mu_B}{\hbar} g_{F'=2} B_z - \frac{\mu_B}{\hbar} g_{F=2} B_z. \quad (\text{S17})$$

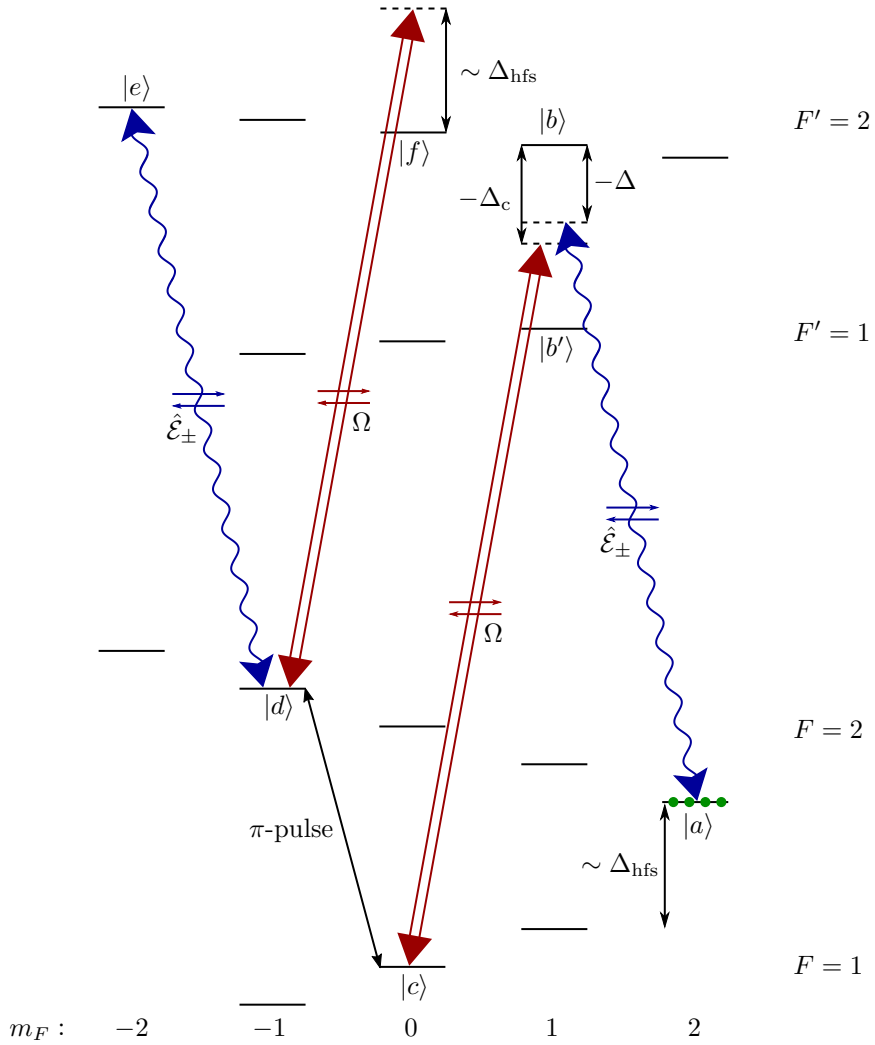


FIG. S5. Implementation of the Λ -type scheme on the D₁ line of ^{87}Rb [S6]. The manifolds $F = 1$ and $F = 2$ belong to the ground state $5^2S_{1/2}$, and the manifolds $F' = 1$ and $F' = 2$ belong to the excited state $5^2P_{1/2}$. The m_F -levels in each manifold are split by the applied magnetic field. The detunings Δ and Δ_c are shown with a minus sign to make their definition consistent with Fig. 1(a) of the main article and illustrate the case when $\Delta, \Delta_c < 0$. The energy splittings are not drawn to scale. During scattering, we assume $|\Delta_{\text{hfs}}| \gg |\Delta|, |\Delta_c|$. During storage and retrieval, we assume $\Delta = \Delta_c = 0$. Atoms are assumed to be pumped into the $F = 2, m_F = 2$ level ($|a\rangle$) before the beginning of the protocol (shown by the green circles on this level). During the EIT storage, the incident photon is stored in the $F = 1, m_F = 0$ level ($|c\rangle$). After a microwave π -pulse, this excitation is transferred to the $F = 2, m_F = -1$ level ($|d\rangle$). Together with the $F' = 2, m_{F'} = -2$ level ($|e\rangle$), this constitutes a two-level atom that provides the optical non-linearity. The classical drive that creates stationary light will also couple the $F = 2, m_F = -1$ level ($|d\rangle$) to the $F' = 2, m_{F'} = 0$ ($|f\rangle$) level with a detuning approximately equal to Δ_{hfs} .

Solving Eqs. (S16) and (S17) with $g_{F'=2} = 1/6$ and $g_{F=2} = 1/2$ [S6] gives

$$\Delta_a = \frac{1}{6} \frac{\mu_B B_z}{\hbar}, \quad (\text{S18})$$

$$\Delta = \frac{\mu_B B_z}{\hbar}. \quad (\text{S19})$$

To determine the time for the π -pulse transferring state $|c\rangle$ to state $|d\rangle$ (see more discussion in Sec. 8), we need to find the splitting of state $|d\rangle$ ($F = 2, m_F = -1$) from the adjacent state with $F = 2, m_F = 0$. This splitting is

$$\Delta_{|F=2, m_F=-1\rangle} - \Delta_{|F=2, m_F=0\rangle} = -\frac{1}{2} \frac{\mu_B B_z}{\hbar} = -\frac{1}{2} \Delta. \quad (\text{S20})$$

To provide a numerical example for the required magnetic field, we can assume $\Gamma_{1D}/\Gamma = 0.05$ and $N = 10^4$. This gives an optimal detuning $\Delta \approx \Delta_c \approx -\sqrt{(\Gamma_{1D}^2 N^{3/2})/(8\pi)} \approx -10\Gamma$. Since $\Gamma = 2\pi \cdot 5.75$ MHz for the D_1 line [S6], the required magnetic field is $B_z = \hbar\Delta/\mu_B \approx -41$ G.

Due to the use of the extreme m_F -level for state $|a\rangle$ (see Fig. S5), it is not coupled to any excited states in the D_1 line by the classical drive, suppressing four-wave mixing noise [S7]. There is, however, a possible drawback of this level structure [S8]: reduction of the effective coupling strength of the $|a\rangle \leftrightarrow |c\rangle$ transition due to the fact that state $|a\rangle$ is also coupled to the excited state $F' = 2$, $m_{F'} = 1$ ($|b'\rangle$). This reduction happens due to the destructive interference of the paths $|a\rangle \leftrightarrow |b\rangle \leftrightarrow |c\rangle$ and $|a\rangle \leftrightarrow |b'\rangle \leftrightarrow |c\rangle$ if the detuning of the probe field from transitions $|a\rangle \leftrightarrow |b\rangle$ and $|a\rangle \leftrightarrow |b'\rangle$ has the same sign. Hence, one has to make sure that the fields are either resonant with one of the transitions (the case during storage and retrieval) or that the detunings have different signs (as shown in Fig. S5). The latter can be satisfied for scattering, if $|\Delta|$ is smaller than the splitting of $|b\rangle$ and $|b'\rangle$. Since the latter splitting is $\sim 100\Gamma$ [S6], the condition is easily satisfiable for e.g. $\Gamma_{1D}/\Gamma = 0.05$ and $N = 10^4$, where $\Delta \approx -10\Gamma$ (for optimal fidelity). Even though the above approach suppresses the noise during EIT storage and retrieval, the presence of the classical drive can still induce noise during scattering due to the off-resonant coupling of state $|d\rangle$ to state $|f\rangle$ (see Fig. S5). See Sec. 7 below for a discussion of this coupling.

Finally, we note that by setting the two counter-propagating classical drives at different frequencies such that they have detunings Δ_{c+} and Δ_{c-} (we are only interested in the off-resonant case, i.e. $\Delta_{c+}, \Delta_{c-} \neq 0$), this setup becomes an implementation of a dual-color scheme [S9]. This scheme is equivalent to the dual-V [S10] scheme discussed in the main article, if [S11]

$$|\Delta_{c+} - \Delta_{c-}| < \frac{|\Delta_{c+} + \Delta_{c-}|}{2} \quad (\text{S21})$$

(i.e. splitting between the two frequencies is smaller than their average magnitude), and

$$|\Delta_{c+} - \Delta_{c-}| \gtrsim \frac{|\Omega_0|^2}{|\Delta_{c+} + \Delta_{c-}|} \quad (\text{S22})$$

(i.e. splitting between the two frequencies is bigger than the ac Stark shift induced by the classical drives). These two conditions set additional restrictions on the Rabi frequency and, in particular, may require the gate time (dominated by the scattering time $(\Gamma_{1D}^{3/2} N^{7/4})/(4\pi^{3/2} \sqrt{\Gamma'} |\Omega_0|^2)$ derived in Sec. 9 below) to be longer for the dual-color scheme than for the Λ -type scheme. E.g. for $\Gamma_{1D}/\Gamma = 0.05$ and $N = 10^4$, $|\Delta_{c+} + \Delta_{c-}|/2 \approx 10\Gamma$ needs to be chosen for optimal fidelity. From Eqs. (S21) and (S22), we thus have $|\Omega_0| \lesssim 10\Gamma$. A full investigation of this is beyond the scope of the present analysis.

3. FIDELITY

Here, we state the expressions required for evaluating the Choi-Jamiolkowski fidelity and success probability accounting for non-zero bandwidth of the scattered photon B . We will also discuss, how the unconditional and conditional fidelities are related to figures of merit for quantum repeaters. A more detailed discussion can be found in Refs. [S12, S13].

The ideal evolution of the controlled-phase gate is defined by its action on the computational basis states

$$|00\rangle_{\text{in}} \rightarrow |00\rangle_{\text{out}}, \quad (\text{S23})$$

$$|01\rangle_{\text{in}} \rightarrow |01\rangle_{\text{out}}, \quad (\text{S24})$$

$$|10\rangle_{\text{in}} \rightarrow |10\rangle_{\text{out}}, \quad (\text{S25})$$

$$|11\rangle_{\text{in}} \rightarrow -|11\rangle_{\text{out}}. \quad (\text{S26})$$

To calculate the Choi-Jamiolkowski fidelity, we have to define the input basis states ($|jj'\rangle_{\text{in}}$ for $j, j' \in \{0, 1\}$) and their ideal evolution into the output states ($|jj'\rangle_{\text{out}}$). Since photon A is stored and retrieved, and photon B is scattered, it is most natural to describe the former as a temporal wave packet and the latter through a frequency distribution over δ_B , where $\delta_B = \Delta - \Delta_c$ (see Figs. 1(a) and 1(b) of the main article) is the two-photon detuning. We define the ideal evolution such that the output frequency distribution of photon B is equal to the input frequency distribution, and the output wave packet of photon A is set to be the one obtained after storage and retrieval in the absence of scattering. These choices of the ideal output wave functions $\phi_{A,\text{out},0}$ and ϕ_B are natural, but there may exist

more optimal choices that give better fidelities. In terms of the storage and retrieval kernels, $K_{s,j}(t_A)$ and $K_{r,j}(t_A)$, respectively (discussed in Sec. 6 below), the output wave packet of photon A is

$$\phi_{A,\text{out},0}(t_A) = \sum_j \int K_{r,j}(t_A) K_{s,j}(t'_A) \phi_{A,\text{in}}(t'_A) dt'_A, \quad (\text{S27})$$

where $\phi_{A,\text{in}}$ is the input wave packet. We define $\phi_{A,\text{out},0}$ to be unnormalized, and the absolute square of its norm $\eta_{\text{EIT}} = \int |\phi_{A,\text{out},0}(t_A)|^2 dt_A$ is the EIT storage and retrieval efficiency, which is, in general, less than unity due to imperfections. When defining the output basis states ($|jj'\rangle_{\text{out}}$), we ensure that they are normalized by dividing them by $\sqrt{\eta_{\text{EIT}}}$. In the numerical calculations, we use the discrete definition (S27) of $\phi_{A,\text{out},0}$ (and a similar one for $\phi_{A,\text{out},1}$ below) instead of the continuum version that was stated in the main article for simplicity.

We also need to find the output wave packet for photon A for the case when photon B was scattered from the atomic ensemble while photon A was stored in it. It is

$$\phi_{A,\text{out},1}(t_A, \delta_B) = \sum_j \int K_{r,j}(t_A) R_{1,j}(\delta_B) K_{s,j}(t'_A) \phi_{A,\text{in}}(t'_A) dt'_A. \quad (\text{S28})$$

Note that, compared to $\phi_{A,\text{out},0}$, the reflection coefficient $R_{1,j}(\delta_B)$ appears in the definition. This reflection coefficient depends on the position where photon A was stored, hence it cannot be taken outside of the summation over j . Perfect controlled-phase gate operation (neglecting the bandwidth of photon B) is achieved when $\phi_{A,\text{out},1}(t_A, \delta_{\text{res}}) = -\phi_{A,\text{out},0}(t_A)$ for some δ_{res} .

The Choi-Jamiolkowski fidelity is computed by assuming a particular entangled state as the input and applying both the ideal and real evolution to it [S12–S14]. The fidelity between the output states is then the Choi-Jamiolkowski fidelity. It is given by

$$F_{\text{CJ}} = \frac{\eta_{\text{EIT}}}{16} \left| 2t_b + \int R_0(\delta_B) |\phi_B(\delta_B)|^2 d\delta_B - \frac{1}{\eta_{\text{EIT}}} \iint \phi_{A,\text{out},0}^*(t_A) \phi_{A,\text{out},1}(t_A, \delta_B) |\phi_B(\delta_B)|^2 dt_A d\delta_B \right|^2. \quad (\text{S29})$$

If we neglect the bandwidth of photon B by setting $|\phi_B(\delta_B)|^2$ to be the Dirac delta function, $|\phi_B(\delta_B)|^2 = \delta(\delta_B - \delta_{\text{res}})$, in the above expression, we obtain Eq. (5) of the main article.

The success probability for having two photons at the output is

$$P_{\text{suc}} = \frac{\eta_{\text{EIT}}}{4} \left(2|t_b|^2 + \int |R_0(\delta_B)|^2 |\phi_B(\delta_B)|^2 d\delta_B + \frac{1}{\eta_{\text{EIT}}} \iint |\phi_{A,\text{out},1}(t_A, \delta_B)|^2 |\phi_B(\delta_B)|^2 dt_A d\delta_B \right). \quad (\text{S30})$$

Setting $|\phi_B(\delta_B)|^2 = \delta(\delta_B - \delta_{\text{res}})$, this reduces to Eq. (6) of the main article. The conditional Choi-Jamiolkowski fidelity is $F_{\text{CJ,cond}} = F_{\text{CJ}}/P_{\text{suc}}$.

The abstract Choi-Jamiolkowski fidelity considered above can be related to more concrete figures of merit, such as entanglement swap fidelity and success probability in the setting of quantum repeaters. In Refs. [S12, S13] it is shown that the success probability of the entanglement swap operation (see Fig. 1(c) of the main article and Sec. 1 above) is exactly the same as the success probability P_{suc} defined by Eq. (S30). Furthermore, since F_{CJ} measures the probability of the photons to be in the right modes with the right phase, whereas P_{suc} measures whether the photons are coming out, it holds that $F_{\text{CJ}} \leq P_{\text{suc}}$. The expressions for F_{CJ} stated in the main article thus give a lower bound for P_{suc} . For our particular implementation of the controlled-phase gate, most of the error in F_{CJ} is caused by photon loss, and hence we have $F_{\text{CJ}} \approx P_{\text{suc}}$. At the same time, $F_{\text{CJ,cond}}$ is a lower bound and an approximation for the entanglement swap fidelity F_{swap} [S12, S13]. In Fig. S6, we illustrate the approximate equalities of F_{CJ} with P_{suc} and $F_{\text{CJ,cond}}$ with F_{swap} .

4. SCATTERING COEFFICIENTS FOR THE ENSEMBLE

4.1. Transfer matrix formalism

To find the scattering coefficients for an ensemble of Λ -type atoms, the single-mode transfer matrix formalism [S15] is sufficient. For the dual-V scheme, two different polarization modes of the electric field are coupled to the atoms, and hence a generalization to a two-mode transfer matrix formalism is required. The general multi-mode transfer matrix

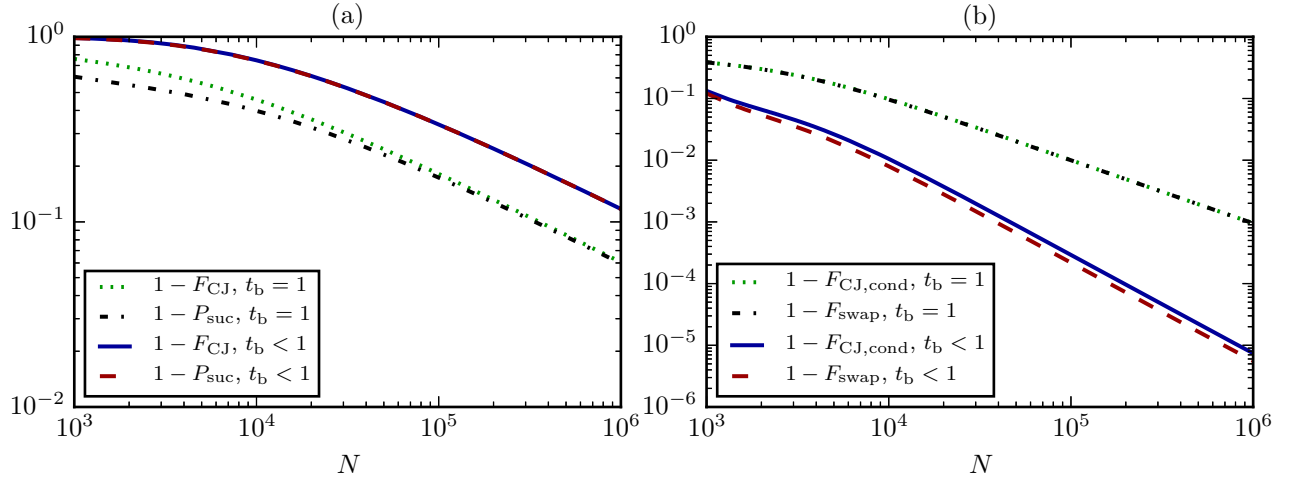


FIG. S6. (a) Comparison of the Choi-Jamiolkowski fidelity F_{CJ} for deterministic operation of the controlled-phase gate with the success probability P_{suc} for heralded operation of the gate. (b) Comparison of the conditional Choi-Jamiolkowski fidelity $F_{\text{CJ,cond}}$ with the entanglement swap fidelity F_{swap} for heralded operation of the gate. For both (a) and (b), Λ -type scheme is used, but the comparison for the dual-V scheme is similar. Dotted green and dash-dotted black curves are calculated with $t_b = 1$, and the solid blue and dashed red curves are calculated with t_b chosen such that the entanglement swap fidelity F_{swap} is maximal. All quantities are plotted as functions of the number of atoms N with fixed $\Gamma_{1D}/\Gamma = 0.05$ and $\Omega_0/\Gamma = 1$. Under EIT (storage and retrieval), $\Omega(z) = \Omega_0$. Under stationary light (scattering), $\Omega(z) = \Omega_0 \cos(k_0 z)$. For storage and retrieval, we use the discretized continuum storage and retrieval kernels discussed in Sec. 6.4.

formalism is developed in Ref. [S11]. Here, we briefly summarize it before applying it to calculate the scattering coefficients of atomic ensembles.

In the multi-mode transfer matrix formalism, electric fields are described by vectors of $2n_m$ elements, where n_m is the number of the different modes of the electric field. The fields propagating to the right and the fields propagating to the left are treated as being distinct, hence there are n_m elements for each propagation direction. We can write the electric field vectors

$$\mathbf{E}(z) = \begin{pmatrix} \mathbf{E}_+(z) \\ \mathbf{E}_-(z) \end{pmatrix}, \quad (\text{S31})$$

where \mathbf{E}_+ is the part of the electric field that propagates to the right (in the positive direction), \mathbf{E}_- is the part of the electric field that propagates to the left (in the negative direction).

Atoms and free propagation between atoms are described by $2n_m \times 2n_m$ matrices that relate the vectors of electric field at one position to vectors of electric field at a different position. In general, the transfer matrix for the whole ensemble is obtained by multiplying the transfer matrices for the atoms and free propagation. We use this approach for the dual-V atoms, for which we assume a placement of the atoms that is incommensurate with the wavelength of the classical drives (or even completely random). For the Λ -type scheme, the atoms are regularly placed with distance $d = \pi/(2k_0)$, as shown in Fig. S7. Hence, the ensemble consists of repeated unit cells, and one can instead exponentiate the transfer matrix for a single unit cell to find the transfer matrix for the whole ensemble. For Λ -type atoms described by 2×2 transfer matrices, closed-form expression can be obtained for the transfer matrix for the whole ensemble given in terms of the transfer matrix for the unit cell [S11]. If the transfer matrix for the unit cell is

$$T_{\text{cell}} = \begin{pmatrix} T_{11} & T_{12} \\ T_{21} & T_{22} \end{pmatrix} \quad (\text{S32})$$

then the transfer matrix for an ensemble of n such unit cells is

$$T_{\text{cell}}^n = e^{in\theta A} = (\cos n\theta)I + i(\sin n\theta)A \quad (\text{S33})$$

where I is the identity matrix,

$$A = \frac{1}{\sin \theta} \begin{pmatrix} i(T_{22} - T_{11})/2 & -iT_{12} \\ -iT_{21} & -i(T_{22} - T_{11})/2 \end{pmatrix}, \quad (\text{S34})$$

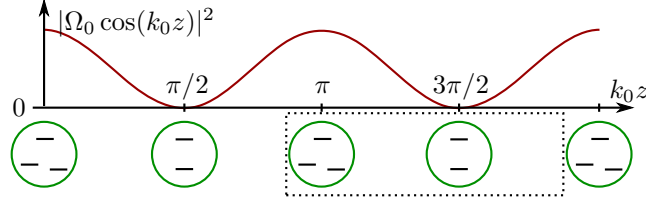


FIG. S7. Standing wave of the Rabi frequency of classical drive for the Λ -type scheme. The circles with 2 or 3 energy levels below the plot represent how the atoms will effectively behave in the different positions, i.e. either as two-level atoms on the nodes or as Λ -type atoms on the anti-nodes. The unit cell is shown by the dotted rectangle.

and θ fulfills $\cos(\theta) = \text{tr}(T_{\text{cell}})/2 = (T_{11} + T_{22})/2$. Physically, θ is equal to the Bloch vector q multiplied by the length occupied by the unit cell. In the case of the Λ -type scheme with inter-atomic spacing $d = \pi/(2k_0)$ below, the unit cell has length $2d$ and hence we have $\theta = 2qd$.

Once the transfer matrix for the ensemble T_e has been obtained, one needs to extract the scattering coefficients from it. The transfer matrix for the ensemble T_e fulfills the relation

$$\begin{pmatrix} \mathbf{E}_+(L^+) \\ \mathbf{E}_-(L^+) \end{pmatrix} = \begin{pmatrix} T_{e,11} & T_{e,12} \\ T_{e,21} & T_{e,22} \end{pmatrix} \begin{pmatrix} \mathbf{E}_+(0^-) \\ \mathbf{E}_-(0^-) \end{pmatrix}. \quad (\text{S35})$$

For the dual-V atoms, the parts \mathbf{E}_\pm have two elements, corresponding to the two polarizations (σ_+ and σ_-). To calculate the reflection coefficient of the ensemble, when the field is incident from the left, we assume input fields

$$\mathbf{E}_+(0^-) = \begin{pmatrix} 1 \\ 0 \end{pmatrix}, \quad \mathbf{E}_-(L^+) = \begin{pmatrix} 0 \\ 0 \end{pmatrix} \quad (\text{S36})$$

(i.e. only a right-moving σ_+ field incident from the left). Then from Eq. (S35) we see that

$$\mathbf{E}_-(0^-) = -T_{e,22}^{-1} T_{e,12} \mathbf{E}_+(0^-), \quad (\text{S37})$$

$$\mathbf{E}_+(L^+) = (T_{e,11} - T_{e,12} T_{e,22}^{-1} T_{e,21}) \mathbf{E}_+(0^-). \quad (\text{S38})$$

The first (σ_+) element of $\mathbf{E}_+(L^+)$ is the transmission coefficient t_e , and the second (σ_-) element of $\mathbf{E}_-(0^-)$ is the reflection coefficient r_e . In the single-mode case, the reflection and transmission coefficients simplify to $r_e = -T_{e,21}/T_{e,22}$ and $t_e = 1/T_{e,22}$, respectively. Note that this result gives a full description of the scattering problem including possible phase shifts induced by the scattering [S16].

The only thing left to describe in the general case, is how the matrix T_{cell} (and T_e if it is not simply equal to T_{cell}^n) is calculated. It is a product of the matrices $T_a(\beta)$ describing scattering of the electric fields by the atoms and the matrices $T_f(k_0d)$ describing the free propagation of the electric fields. They are given by

$$T_a(\beta) = \begin{pmatrix} I - \beta & -\beta \\ \beta & I + \beta \end{pmatrix}, \quad T_f(k_0d) = \begin{pmatrix} e^{ik_0d} I & 0 \\ 0 & e^{-ik_0d} I \end{pmatrix}, \quad (\text{S39})$$

where I means the $n_m \times n_m$ identity matrix (a scalar equal to unity in the single-mode case), k_0 is the wave vector, and d is the propagation distance. Each matrix $T_a(\beta)$ is given in terms a $n_m \times n_m$ matrix β that will be defined for the specific cases of Λ -type and dual-V atoms considered below.

4.2. Reflection and transmission for the Λ -type scheme

4.2.1. Without a stored photon

Here, we derive the scattering coefficients r_0 and t_0 given by Eqs. (1) and (2) of the main article. For the Λ -type atoms, we use single-mode transfer matrices, and hence the parameter β in Eq. (S39) is a scalar. We consider a unit cell that consists of two atoms and two lengths of free propagation (see Fig. S7). One of the atoms is placed on the

anti-node of the standing wave of the classical drive, and the other is placed on the node. The scattering from the former is described by the parameter [S11]

$$\beta_3 = \frac{\Gamma_{1D}\delta}{(\Gamma' - 2i\Delta)\delta + 2i|\Omega_0|^2}, \quad (\text{S40})$$

and the scattering for the latter (an effective two-level atom) is described by the parameter

$$\beta_2 = \frac{\Gamma_{1D}}{\Gamma' - 2i\Delta}. \quad (\text{S41})$$

The transfer matrix for the unit cell is

$$T_{\text{cell}} = T_f(\pi/2)T_a(\beta_2)T_f(\pi/2)T_a(\beta_3). \quad (\text{S42})$$

Carrying out the above matrix multiplications results in

$$T_{\text{cell}} = \begin{pmatrix} -(1-\beta_2)(1-\beta_3) - \beta_2\beta_3 & \beta_3(1-\beta_2) - \beta_2(1+\beta_3) \\ \beta_2(1-\beta_3) - \beta_3(1+\beta_2) & -\beta_2\beta_3 - (1+\beta_2)(1+\beta_3) \end{pmatrix}. \quad (\text{S43})$$

From Eq. (S33), we then have

$$T_e = T_{\text{cell}}^n = \cos(n\theta) \begin{pmatrix} 1 & 0 \\ 0 & 1 \end{pmatrix} + \frac{\sin(n\theta)}{\sin(\theta)} \begin{pmatrix} \beta_2 + \beta_3 & -\beta_2 + \beta_3 - 2\beta_2\beta_3 \\ \beta_2 - \beta_3 - 2\beta_2\beta_3 & -\beta_2 - \beta_3 \end{pmatrix} \quad (\text{S44})$$

with θ given by $\cos(\theta) = \text{tr}(T_{\text{cell}})/2 = -1 - 2\beta_2\beta_3$. From this matrix, we obtain the reflection and transmission coefficients

$$r_0 = -\frac{T_{e,21}}{T_{e,22}} = \frac{-\beta_2 + \beta_3 + 2\beta_2\beta_3}{\frac{\cos(n\theta)}{\sin(n\theta)} \sin(\theta) - (\beta_2 + \beta_3)}, \quad (\text{S45})$$

$$t_0 = \frac{1}{T_{e,22}} = \frac{1}{\cos(n\theta) - \frac{\sin(n\theta)}{\sin(\theta)}(\beta_2 + \beta_3)}. \quad (\text{S46})$$

The minima of r_0 and maxima of t_0 (see Fig. 2 of the main article) occur when $\sin(n\theta)$ in Eq. (S44) is approximately equal to zero. However, exact equality is never satisfied, since θ is complex (a consequence of $\Gamma' > 0$). In the regime where losses are small ($\text{Im}[\text{tr}(T_{\text{cell}})] \ll 1$), the approximate resonance condition is

$$\sin(n \arccos(\text{Re}[\text{tr}(T_{\text{cell}})]/2)) = 0. \quad (\text{S47})$$

In the coefficients (S45) and (S46) we can approximate

$$\theta = \arccos(\text{tr}(T_{\text{cell}})/2) \approx \arccos(\text{Re}[\text{tr}(T_{\text{cell}})]/2) - \frac{i \text{Im}[\text{tr}(T_{\text{cell}})]/2}{\sqrt{(1 - \text{Re}[\text{tr}(T_{\text{cell}})]/2)(1 + \text{Re}[\text{tr}(T_{\text{cell}})]/2)}}. \quad (\text{S48})$$

From Eq. (S47) we have

$$n \arccos(\text{Re}[\text{tr}(T_{\text{cell}})]/2) = \pi k \quad (\text{S49})$$

for some integer k . Since we are interested in the first reflection minimum closest to $\delta = 0$, we choose $k = n - 1$. For large n , we have

$$\text{Re}[\text{tr}(T_{\text{cell}})]/2 = \cos(\pi(n-1)/n) \approx -1 + \pi^2/(2n^2). \quad (\text{S50})$$

Hence, Eq. (S48) can be approximated

$$\theta \approx \pi(n-1)/n - in \text{Im}[\text{tr}(T_{\text{cell}})]/(2\pi), \quad (\text{S51})$$

and we also obtain the approximate expressions:

$$\sin(n\theta) \approx (-1)^{n-1} \left(-in^2 \text{Im}[\text{tr}(T_{\text{cell}})]/(2\pi) \right), \quad (\text{S52})$$

$$\cos(n\theta) \approx (-1)^{n-1}, \quad (\text{S53})$$

$$\sin(\theta) \approx \pi/n. \quad (\text{S54})$$

With these approximations and using the fact that $\text{Im}[\text{tr}(T_{\text{cell}})] = -4 \text{Im}[\beta_2\beta_3]$, Eqs. (S45) and (S46) become

$$r_0 \approx \frac{-\beta_2 + \beta_3 + 2\beta_2\beta_3}{-\frac{i\pi^2}{2n^3 \text{Im}[\beta_2\beta_3]} - \beta_2 - \beta_3}, \quad (\text{S55})$$

$$t_0 \approx \frac{(-1)^{n-1}}{1 - \frac{2in^3 \text{Im}[\beta_2\beta_3]}{i\pi^2}(\beta_2 + \beta_3)}. \quad (\text{S56})$$

To determine the dominant terms in Eqs. (S55) and (S56), we write the approximate expressions for Eqs. (S40) and (S41) in the limit where δ is small, and $|\Delta_c|$ is large ($\Delta = \Delta_c + \delta$). We thereby get

$$\beta_3 \approx -i \frac{\Gamma_{1D}\delta}{2|\Omega_0|^2}, \quad (\text{S57})$$

$$\beta_2 \approx i \frac{\Gamma_{1D}}{2\Delta} + \frac{\Gamma_{1D}\Gamma'}{4\Delta^2}. \quad (\text{S58})$$

The second term on the right hand side of Eq. (S58) is included, since it is the lowest order term in $\text{Re}[\beta_2]$. The latter is used for finding an approximation for $\text{Im}[\beta_2\beta_3] \approx \text{Re}[\beta_2] \text{Im}[\beta_3]$. An expression for the detuning δ can be found using Eq. (S50). Expanding its left hand side to second order in δ around 0, results in the quadratic equation that determines the two-photon detuning $\delta = \delta_{\text{res}}$ of the transmission resonance nearest $\delta = 0$,

$$\frac{\Gamma_{1D}^2}{2\Delta_c|\Omega_0|^2} \delta_{\text{res}} - \frac{\Gamma_{1D}^2(|\Omega_0|^2 - \Delta_c^2)}{2\Delta_c^2|\Omega_0|^4} \delta_{\text{res}}^2 + \frac{\pi^2}{2n^2} = 0. \quad (\text{S59})$$

We choose the solution of this equation where δ_{res} and Δ_c have opposite signs (we assume $\delta_{\text{res}} > 0$ and $\Delta_c < 0$, but the opposite case should also work), i.e.

$$\frac{\delta_{\text{res}}}{|\Omega_0|^2} = \frac{\Delta_c \left(-\Gamma_{1D} + \sqrt{\Gamma_{1D}^2 - 4(\Delta_c^2 - |\Omega_0|^2)\pi^2/n^2} \right)}{2\Gamma_{1D}(\Delta_c^2 - |\Omega_0|^2)} \quad (\text{S60})$$

In the limit of large n , we find

$$\frac{\delta_{\text{res}}}{|\Omega_0|^2} \approx -\frac{\pi^2 \Delta_c}{\Gamma_{1D}^2 n^2} - \frac{\pi^4 \Delta_c^3}{\Gamma_{1D}^4 n^4} + \frac{\pi^4 \Delta_c |\Omega_0|^2}{\Gamma_{1D}^4 n^4}. \quad (\text{S61})$$

The first term on the right hand side of Eq. (S61) could also be derived using the quadratic approximation of the dispersion relation, i.e. $\delta \approx (1/2m)(qd)^2 = (1/2m)(\theta d/2)^2$ with the effective mass $m = -\Gamma_{1D}^2/(8(\Delta_c + i\Gamma'/2)|\Omega_0|^2)$ [S11], but the other two terms result from higher order corrections to this approximation. The resonance detuning $\delta_{\text{res}} \approx -4\pi^2 \Delta_c |\Omega_0|^2 / (\Gamma_{1D}^2 N^2)$ that is quoted in the main article results from only keeping the first term on the right hand side of Eq. (S61) and using $N = 2n$.

When we calculate the fidelity F_{CJ} in Sec. 9 below, we find that it is maximal for a detuning

$$|\Delta_c| \propto \Gamma_{1D} n^{3/4}. \quad (\text{S62})$$

If we insert this expression into (S61), we find that the first term on the right hand side is proportional to $n^{-5/4}$, and the second one is proportional to $n^{-7/4}$. Hence, the second one is smaller for large n and can be neglected. We keep the third term, since it depends on Ω_0 and will be important when accounting for the non-zero bandwidth of the scattered photon.

Using only the first term in Eq. (S61) and inserting (i.e. setting $\Delta = \Delta_c + \delta_{\text{res}}$) it into the first term of Eq. (S58), we find

$$\beta_2 \approx \text{Im}[\beta_2] \approx i \frac{\Gamma_{1D}}{2\Delta_c \left(1 - (\pi^2 |\Omega_0|^2) / (\Gamma_{1D}^2 n^2) \right)} \approx i \frac{\Gamma_{1D}}{2\Delta_c} + i \frac{\pi^2 |\Omega_0|^2}{2\Delta_c \Gamma_{1D} n^2}. \quad (\text{S63})$$

Inserting into the second term of Eq. (S58) gives

$$\text{Re}[\beta_2] \approx \frac{\Gamma_{1D}\Gamma'}{4\Delta_c^2 \left(1 - (\pi^2 |\Omega_0|^2) / (\Gamma_{1D}^2 n^2) \right)^2} \approx \frac{\Gamma_{1D}\Gamma'}{4\Delta_c^2} + \frac{\pi^2 \Gamma' |\Omega_0|^2}{2\Delta_c^2 \Gamma_{1D} n^2}. \quad (\text{S64})$$

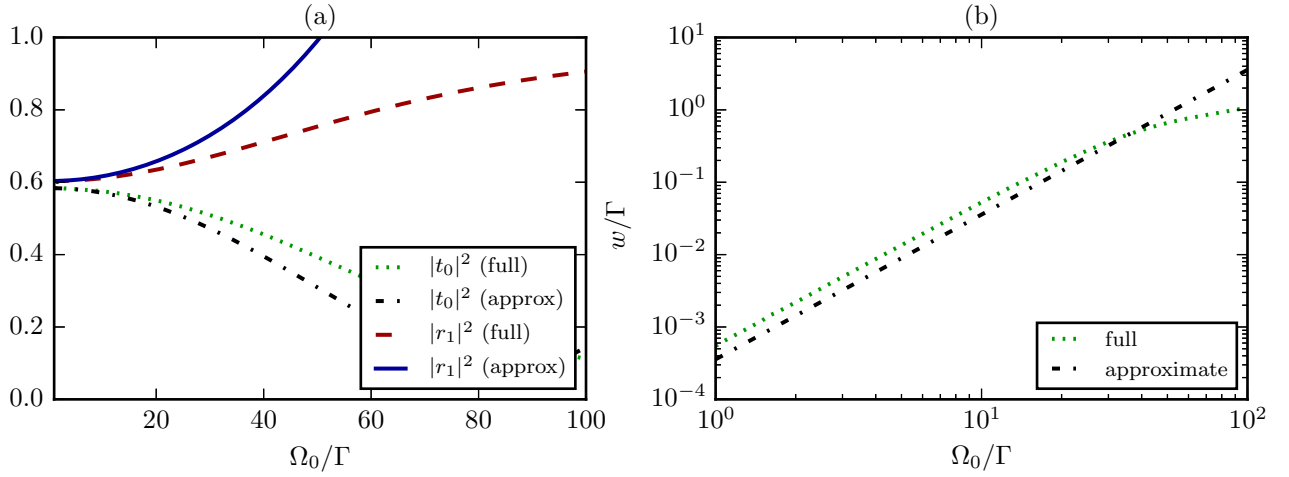


FIG. S8. (a) Reflectance with a stored photon $|r_1|^2$ and transmittance without a stored photon $|t_0|^2$ of an ensemble of Λ -type atoms plotted as functions of the Rabi frequency of the classical drive Ω_0 and evaluated at the transmission resonance closest to $\delta = 0$ (see Fig. 2 of the main article), i.e. at $\delta = \delta_{\text{res}}$. Both t_0 and r_1 are calculated either numerically by directly using Eqs. (S46) and (S74), respectively (“full”), or from the approximate expressions in Eqs. (S68) and (S80), respectively (“approx”). For the approximate expressions, the curves are shifted such that the values for $\Omega_0 = 0$ are the same for both the full and approximate curves. This is done to show the dependency on Ω_0 more clearly. For the unshifted curves, there is still visible difference even for $\Omega_0 = 0$. This difference disappears as N increases (and Δ_c is changed accordingly). (b) The width of the transmission resonance calculated either from the full expression as $w = \text{Re} \left[\sqrt{4/\partial_\delta^2 t_0(\delta)} \right] \Big|_{\delta=\delta_{\text{res}}}$ or using the approximate expression (S70) (dash-dotted black). The parameters for both (a) and (b) are: $N = 10^4$, $\Gamma_{1D}/\Gamma = 0.05$, and $\Delta_c/\Gamma = -10$. (The same as in Fig. 2 of the main article except for Ω_0 that is varied here.)

Using the first and the third terms of Eq. (S61) and inserting them into Eq. (S57), we find

$$\beta_3 \approx \text{Im}[\beta_3] \approx -i \frac{\Gamma_{1D}}{2} \left(-\frac{\pi^2 \Delta_c}{\Gamma_{1D}^2 n^2} + \frac{\pi^4 \Delta_c |\Omega_0|^2}{\Gamma_{1D}^4 n^4} \right) \approx i \frac{\pi^2 \Delta_c}{2\Gamma_{1D} n^2} - i \frac{\pi^4 \Delta_c |\Omega_0|^2}{2\Gamma_{1D}^3 n^4}. \quad (\text{S65})$$

Combining Eqs. (S64) and (S65) and neglecting a term of order n^{-6} results in

$$\text{Im}[\beta_2 \beta_3] \approx \text{Re}[\beta_2] \text{Im}[\beta_3] \approx \frac{\pi^2 \Gamma'}{8\Delta_c n^2} + \frac{\pi^4 \Gamma' |\Omega_0|^2}{8\Delta_c \Gamma_{1D}^2 n^4}. \quad (\text{S66})$$

Invoking Eq. (S62) again and neglecting the Ω_0 dependent terms for a moment, we see that $\beta_2 \propto n^{-3/4}$, $\beta_3 \propto n^{-5/4}$ and $n^3 \text{Im}[\beta_2 \beta_3] \propto n^{1/4}$. Hence, $\beta_3 \ll \beta_2$; $\beta_2, \beta_3 \ll (n^3 \text{Im}[\beta_2 \beta_3])^{-1}$, and we can approximate Eqs. (S55) and (S56) (now including the Ω_0 dependent terms) by

$$r_0 \approx -i \frac{2n^3}{\pi^2} \beta_2 \text{Im}[\beta_2 \beta_3] \approx \frac{\Gamma_{1D} \Gamma' n}{8\Delta_c^2} + \frac{\pi^2 \Gamma' |\Omega_0|^2}{4\Delta_c^2 \Gamma_{1D} n}, \quad (\text{S67})$$

$$t_0 \approx (-1)^{n-1} \left(1 + i \frac{2n^3}{\pi^2} \beta_2 \text{Im}[\beta_2 \beta_3] \right) \approx (-1)^{n-1} \left(1 - \frac{\Gamma_{1D} \Gamma' n}{8\Delta_c^2} - \frac{\pi^2 \Gamma' |\Omega_0|^2}{4\Delta_c^2 \Gamma_{1D} n} \right). \quad (\text{S68})$$

Since the number of atoms is $N = 2n$, the above expressions correspond to Eqs. (1) and (2) of the main article, except for the removal of the overall phase factor $(-1)^{n-1}$ for the transmission coefficient t_0 (discussed in Sec. 5 below) and ignoring the shown Ω_0 dependent terms (they get canceled in the fidelity calculations in Sec. 9 below). In Fig. S8(a) we plot $|t_0|^2$ as a function of Ω_0 and show that the approximate analytical expression in Eq. (S68) matches the full expression in Eq. (S46) evaluated at the resonance frequency δ_{res} (found numerically).

To account for the non-zero bandwidth of the scattered photon, we also need the width of the resonance. After expanding the reflection coefficient r_0 around δ_{res} , we get

$$r_0(\delta) \approx (2/w^2)(\delta - \delta_{\text{res}})^2 + r_0(\delta_{\text{res}}), \quad (\text{S69})$$

where $r_0(\delta_{\text{res}})$ is given by Eq. (S67) and

$$w = \frac{32\sqrt{2}\pi^2\Delta_c^2|\Omega_0|^2}{\Gamma_{1D}^3 N^3}, \quad (\text{S70})$$

is the width. Since $t_0 \approx 1 - r_0$, the width of the transmission resonance is w . In Fig. S8(b), we compare Eq. (S70) with the numerically computed width.

4.2.2. With a stored photon

Here, we derive the scattering coefficients r_1 and t_1 given by Eqs. (3) and (4) of the main article. The starting point is the assumption that the photon has been stored in a single atom that is placed at the anti-node of the standing wave of the classical drive (storing in an atom that is on the node will have a negligible change in the scattering properties, unless Γ_{1D}/Γ is close to unity). The storage of a photon in the atom transfers it from state $|a\rangle$ to state $|d\rangle$, such that it behaves like a resonant two-level atom (given by the $|d\rangle \leftrightarrow |e\rangle$ transition) that is described by the transfer matrix $T_a(\beta_{2,de})$ with

$$\beta_{2,de} = \frac{\Gamma_{1D}}{\Gamma'}. \quad (\text{S71})$$

Hence, the transfer matrix for the unit cell containing the stored photon is

$$T_{\text{cell,ph}} = T_f(\pi/2)T_a(\beta_2)T_f(\pi/2)T_a(\beta_{2,de}), \quad (\text{S72})$$

instead of Eq. (S42). If we assume that the photon is stored in the unit cell with index n_{ph} , the transfer matrix for the whole ensemble $T_{e,n_{\text{ph}}}$ is given by

$$T_{e,n_{\text{ph}}} = T_{\text{cell}}^{n-n_{\text{ph}}} T_{\text{cell,ph}} T_{\text{cell}}^{n_{\text{ph}}-1}. \quad (\text{S73})$$

From Eq. (S73) we can find the scattering coefficients as

$$r_{1,n_{\text{ph}}} = -\frac{T_{e,n_{\text{ph}},21}}{T_{e,n_{\text{ph}},22}}, \quad (\text{S74})$$

$$t_{1,n_{\text{ph}}} = \frac{1}{T_{e,n_{\text{ph}},22}}, \quad (\text{S75})$$

where $T_{e,n_{\text{ph}},jj'}$ are the elements of the matrix $T_{e,n_{\text{ph}}}$.

For the numerical calculations, Eqs. (S74) and (S75) are used directly. For the analytical calculations, we can find approximate expressions for the scattering coefficients, but the procedure is rather involved. We shall therefore restrict ourselves to a brief discussion of the main steps. We do several simplifications on the (very complicated) expressions resulting from Eqs. (S74) and (S75). We use the fact that $\beta_2\beta_3 = (-1 - \cos(\theta))/2$ and the approximate expression $\theta \approx \pi(n-1)/n$. Also, while expanding the numerator and denominator around large n , we use that $\beta_2 \propto n^{-3/4}$ (a consequence of Eqs. (S41) and (S62)) to determine which terms can be neglected. Then we replace the index of the unit cell with the stored photon n_{ph} by $n\tilde{z}$, where $\tilde{z} = z/L$ is the rescaled position coordinate. After further approximating $1/n \approx 0$ and $n \pm 1 \approx n$, we get

$$r_1(\tilde{z}) = -\frac{\beta_{2,de}(\pi \cos(\pi\tilde{z}) - 2\beta_2 n \sin(\pi\tilde{z}))^2}{\sin^2(\pi\tilde{z}) (\pi^2 - 4\beta_2^2\beta_{2,de}n^2) - 2\pi\beta_2^2\beta_{2,de}n \sin(2\pi\tilde{z}) + \pi^2(\beta_{2,de} + 1) \cos^2(\pi\tilde{z})}, \quad (\text{S76})$$

$$t_1(\tilde{z}) = \frac{(-1)^{n-1}\pi^2}{\sin^2(\pi\tilde{z}) (\pi^2 - 4\beta_2^2\beta_{2,de}n^2) - 2\pi\beta_2^2\beta_{2,de}n \sin(2\pi\tilde{z}) + \pi^2(\beta_{2,de} + 1) \cos^2(\pi\tilde{z})}. \quad (\text{S77})$$

Next, we insert the expressions for β_2 and $\beta_{2,de}$ with the approximation $\Delta \approx \Delta_c$, expand around $\tilde{z} = 1/2$, and use $|\Delta_c| \propto \Gamma_{1D}n^{3/4}$ to identify which terms are dominant for large n . This results in

$$r_1(\tilde{z}) \approx 1 - \frac{\pi^2\Delta_c^2\Gamma'}{\Gamma_{1D}^3n^2} - \frac{2i\pi^2\Delta_c}{\Gamma_{1D}n} \left(\tilde{z} - \frac{1}{2}\right) - \frac{\pi^4\Delta_c^2(2\Gamma_{1D} + \Gamma')}{\Gamma_{1D}^3n^2} \left(\tilde{z} - \frac{1}{2}\right)^2, \quad (\text{S78})$$

$$t_1(\tilde{z}) \approx (-1)^{n-1} \left(\frac{\pi^2\Delta_c^2\Gamma'}{\Gamma_{1D}^3n^2} + \frac{\pi^4\Delta_c^2\Gamma'}{\Gamma_{1D}^3n^3} \left(\tilde{z} - \frac{1}{2}\right) + \frac{\pi^4\Delta_c^2\Gamma'}{\Gamma_{1D}^3n^2} \left(\tilde{z} - \frac{1}{2}\right)^2 \right). \quad (\text{S79})$$

We see that the resulting expressions do not depend on Ω_0 . This is a consequence of approximating $\Delta \approx \Delta_c$. If we use $\Delta = \Delta_c + \delta$ together with Eq. (S61), we find corrections from the dependence on Ω_0 . We only need the first term in Eq. (S61) to find the lowest order correction due to Ω_0 . At $\tilde{z} = 1/2$, and expanding around large n , we have

$$r_1 \approx 1 - \frac{\pi^2 \Delta_c^2 \Gamma'}{\Gamma_{1D}^3 n^2} + \frac{2\pi^4 \Delta_c^2 \Gamma' |\Omega_0|^2}{\Gamma_{1D}^5 n^4}, \quad (\text{S80})$$

$$t_1 \approx (-1)^{n-1} \left(\frac{\Delta_c^2 \pi^2 \Gamma'}{\Gamma_{1D}^3 n^2} - \frac{2\pi^4 \Delta_c^2 \Gamma' |\Omega_0|^2}{\Gamma_{1D}^5 n^4} \right). \quad (\text{S81})$$

In Fig. S8(a), we plot $|r_1|^2$ as a function of Ω_0 and show that the analytical expression in Eq. (S80) matches the full expression in Eq. (S74) evaluated at the resonance frequency. In Eq. (3) of the main article, we include all error terms of Eq. (S78) but ignore Ω_0 dependent error term from Eq. (S80) (since it gets canceled in the fidelity calculations in Sec. 9 below). Likewise, in Eq. (4) of the main article, we include all error terms of Eq. (S79) but ignore the Ω_0 dependent error term from Eq. (S81).

4.3. Reflection and transmission for the dual-V scheme

For the dual-V scheme, we need two-mode (4×4) transfer matrices to describe the σ_+ and σ_- polarized modes. The transfer matrices for the atoms in Eq. (S39) have the form $T_a(\beta_j)$ (j is the index of the atom) where [S11]

$$\beta_j = -(I + S_{j,r})^{-1} S_{j,r}, \quad (\text{S82})$$

and

$$S_{j,r} = \begin{pmatrix} r_{j,++} & r_{j,-+} \\ r_{j,+ -} & r_{j,--} \end{pmatrix}. \quad (\text{S83})$$

In the expressions above, we have used the same convention as in Eqs. (S36), i.e. that the first element of E_{\pm} is the σ_+ component and the second element is the σ_- component. Hence, in Eq. (S83), $r_{j,+ -}$ for example means the reflection coefficient of the process where an incident σ_+ field is reflected also into an outgoing σ_- field. Similarly for the other reflection coefficients.

If the atom is in state $|a\rangle$ (without a stored photon), the elements of $S_{j,r}$ are given by [S11]

$$r_{j,--} = r_{j,++} = -\frac{i(\Gamma_{1D}/2) (\Delta_{\Gamma} \delta - |\Omega_0|^2)}{\Delta_{\Gamma}^2 \delta - 2\Delta_{\Gamma} |\Omega_0|^2}, \quad (\text{S84})$$

$$r_{j,-+} = -\frac{i(\Gamma_{1D}/2) |\Omega_0|^2}{\Delta_{\Gamma}^2 \delta - 2\Delta_{\Gamma} |\Omega_0|^2} e^{2ik_0 z_j}, \quad (\text{S85})$$

$$r_{j,+ -} = -\frac{i(\Gamma_{1D}/2) |\Omega_0|^2}{\Delta_{\Gamma}^2 \delta - 2\Delta_{\Gamma} |\Omega_0|^2} e^{-2ik_0 z_j}, \quad (\text{S86})$$

where $\Delta_{\Gamma} = \Delta + i(\Gamma/2)$. If the atom is in state $|d\rangle$ (with a stored photon), it acts as a resonant V-type atom, and hence the elements of $S_{j,r}$ are given by

$$r_{j,--} = r_{j,++} = -\frac{\Gamma_{1D}}{\Gamma}, \quad (\text{S87})$$

$$r_{j,-+} = r_{j,+ -} = 0. \quad (\text{S88})$$

We only calculate the reflection and transmission coefficients of ensembles of dual-V atoms numerically.

5. SAGNAC INTERFEROMETER AND ADJUSTMENT OF THE PHASES

Here, we calculate the result of scattering from the Sagnac interferometer shown in Fig. 1(d) of the main article. The sequential picture of the scattering is that the incident field on one of the ports is split by the 50:50 beam splitter,

gets scattered by the ensemble, and then the transmitted and reflected parts will again interfere on the same beam splitter. Thus the matrix that relates the outputs to the inputs can be written

$$M_{\text{Sagnac}} = HM_fSM_fH, \quad (\text{S89})$$

where the matrix H describes the beam splitter, the matrix M_f describes the free propagation, and the matrix S describes scattering from the ensemble.

We choose the phases of the beam splitter such that it performs the Hadamard operation on the field, i.e.

$$H = \frac{1}{\sqrt{2}} \begin{pmatrix} 1 & 1 \\ 1 & -1 \end{pmatrix}. \quad (\text{S90})$$

The free propagation matrix is

$$M_f = \begin{pmatrix} e^{ik_0l_1} & 0 \\ 0 & e^{-ik_0l_2} \end{pmatrix}, \quad (\text{S91})$$

where l_1 and l_2 are lengths of propagation from the beam splitter until either end of the ensemble.

The ensemble can, in general, have different transmission and reflection coefficients depending on, whether the field is incident from the left or right. Therefore, we write

$$S = \begin{pmatrix} r_+ & t_+ \\ t_- & r_- \end{pmatrix}, \quad (\text{S92})$$

where r_+ and t_+ are respectively the reflection and transmission coefficients when the field is incident from the left (propagating in the positive direction), and r_- and t_- are respectively the reflection and transmission coefficients when the field is incident from the right (propagating in the negative direction).

Multiplying the matrices, we get

$$M_{\text{Sagnac}} = \frac{1}{2} \begin{pmatrix} r_+e^{2ik_0l_1} + (t_+ + t_-)e^{ik_0(l_1+l_2)} + r_-e^{2ik_0l_2} & r_+e^{2ik_0l_1} - (t_+ - t_-)e^{ik_0(l_1+l_2)} - r_-e^{2ik_0l_2} \\ r_+e^{2ik_0l_1} + (t_+ - t_-)e^{ik_0(l_1+l_2)} - r_-e^{2ik_0l_2} & r_+e^{2ik_0l_1} - (t_+ + t_-)e^{ik_0(l_1+l_2)} + r_-e^{2ik_0l_2} \end{pmatrix}. \quad (\text{S93})$$

For an empty non-rotating Sagnac interferometer where $r_+ = r_- = 0$ and $t_+ = t_- = 1$, we recover the well known result, that light always leaves the port in which it is incident [S17, S18]. Once we have put a scatterer inside the interferometer, this result is still true if $r_+ = r_-$, $t_+ = t_-$, and $l_1 = l_2$. Because the equalities $r_+ = r_-$, $t_+ = t_-$, and $l_1 = l_2$ need not be true, the off-diagonal entries of M_{Sagnac} are, in general, non-zero and describe the leakage of the incident power to the other port of the Sagnac interferometer. However, due to the sequential operation of the gate, this leakage does not introduce any logic errors: since scattering of photon B happens while photon A is stored inside the ensemble, leakage of photon B into the rail that encodes state $|1\rangle_A$ (see Fig. 1(c) of the main article) is separated in time from the subsequent retrieval of photon A and hence can be either absorbed or rerouted along a different path.

Even though the off-diagonal entries of M_{Sagnac} are non-zero in general, they are strongly suppressed in the ideal limit, since e.g. both r_+ and r_- approach the same value (either 1 or 0 depending on whether a photon was stored in the ensemble or not). As a concrete example, for the Λ -type scheme, we can use Eq. (S44) and find

$$r_{0+} = -\frac{T_{e,21}}{T_{e,22}} = \frac{-\beta_2 + \beta_3 + 2\beta_2\beta_3}{\frac{\cos(n\theta)}{\sin(n\theta)} \sin(\theta) - (\beta_2 + \beta_3)}, \quad (\text{S94})$$

$$r_{0-} = \frac{T_{e,12}}{T_{e,22}} = \frac{-\beta_2 + \beta_3 - 2\beta_2\beta_3}{\frac{\cos(n\theta)}{\sin(n\theta)} \sin(\theta) - (\beta_2 + \beta_3)}, \quad (\text{S95})$$

where r_{0+} is the same as r_0 in Eq. (S45), and r_{0-} is the reflection coefficient where the field is incident from the right instead of the left. The difference between Eqs. (S94) and (S95) is only in the sign of the term $2\beta_2\beta_3$ in the numerator. As discussed above Eq. (S67), this term is much smaller than β_2 in the limit of a large number of atoms and has therefore been neglected in Eq. (S67). Hence, Eq. (S67) can serve as an approximate expression for both r_{0+} and r_{0-} . We also note that it can be shown that the transmission coefficient for any 2×2 transfer matrix is independent of whether the field is incident from one side or the other (given by Eq. (S46) for t_0). However, we still account for the possible difference in the scattering coefficients in the numerical calculations (both for 2×2 and 4×4

transfer matrices) by using the matrix element $M_{\text{Sagnac},22}$ from Eq. (S93) to define the scattering coefficients R_1 and R_0 needed in Eqs. (S28) and (S29), i.e.

$$R_0 = -\frac{1}{2} \left(r_{0+} e^{2ik_0 l_1} - (t_{0+} + t_{0-}) e^{ik_0(l_1+l_2)} + r_{0-} e^{2ik_0 l_2} \right), \quad (\text{S96})$$

$$R_1 = -\frac{1}{2} \left(r_{1+} e^{2ik_0 l_1} - (t_{1+} + t_{1-}) e^{ik_0(l_1+l_2)} + r_{1-} e^{2ik_0 l_2} \right), \quad (\text{S97})$$

where the scattering coefficients with “+” in the subscript assume incident photon from the left of the ensemble, and the scattering coefficients with “-” in the subscript assume incident photon from the right of the ensemble. In most of the calculations, we assume that $e^{2ik_0 l_1} = e^{2ik_0 l_2} = e^{ik_0(l_1+l_2)} = 1$. This is satisfied if l_1 and l_2 are integer multiples of the wavelength $2\pi/k_0$. To find the error introduced by l_1 or l_2 deviating from these values, we both do a numerical and an analytical calculation in Sec. 9 below.

Since the distance between the atoms is fixed in our calculations, as we change the number of atoms, we also change the length of the ensemble and consequently also the total round trip length of the Sagnac interferometer. This introduces additional phase factors which need to be accounted for. There is an overall phase factor $(-1)^{n-1}$ in Eqs. (S68), (S79), and (S81) compared with Eqs. (2) and (4) of the main article. This phase factor reflects the fact the ensemble length changes by half a wavelength (i.e. $2d = \pi/k_0$) whenever a unit cell is added to the ensemble. When $r_{0\pm} \approx 0$ and $|t_{0\pm}| \approx 1$, the factor $(-1)^{n-1}$ directly appears as the overall phase of R_0 . Hence, without the adjustment, the ideal value $R_0 = 1$ can only be obtained for odd n . There are similar phase factor considerations for R_1 due to the phase factor of the reflection coefficient r_{1-} (r_{1+} is assumed to be at $z = 0$ and hence does not acquire phase factors with changing ensemble length). To address this issue, we require that the total round trip of the interferometer to be equal to an odd number of half wavelengths and thus independent of the precise atom number. In the calculations, this is accomplished by adding suitable length of free propagation d_{extra} such that $\exp(ik_0(L + l_1 + l_2 + d_{\text{extra}})) = -1$. Experimentally, stabilizing the total length of the interferometer will suffice.

In general (e.g. for the dual-V scheme), we can choose any inter-atomic spacing d that is not a multiple of $\pi/(2k_0)$ (see Fig. S14 below). For this general case, we expect that instead of the overall phase factor $(-1)^{n-1}$, the transmission coefficients have the phase factor $\exp(ik_0 L + \pi)$. As noted above, we remove this phase factor in the calculations by adding a distance of free propagation d_{extra} to the right of the ensemble chosen such that $\exp(ik_0 d_{\text{extra}}) = \exp(-ik_0 L - \pi)$. Multiplying this extra matrix of free propagation modifies the scattering coefficients according to

$$\begin{aligned} r_{0+} &\rightarrow r_{0+}, \\ r_{0-} &\rightarrow r_{0-} \exp(2ik_0 d_{\text{extra}}), \\ t_{0\pm} &\rightarrow t_{0\pm} \exp(ik_0 d_{\text{extra}}). \end{aligned} \quad (\text{S98})$$

The physical interpretation of this mathematical result is that, since the free propagation was added on the right of the ensemble, then reflection for the field incident from the left (r_{0+}) is unaffected, while the reflection coefficient for fields incident from the right (r_{0-}) acquires twice the propagation phase. The transmission coefficients only acquire the propagation phase once.

6. EIT STORAGE AND RETRIEVAL

6.1. Overview

We model the EIT storage and retrieval process in three different ways:

1. Using the dispersion relation (see for instance Ref. [S19] and Sec. 6.2 below).
2. Using the fully discrete theory (see Ref. [S20] and Sec. 6.3 below).
3. Using the storage and retrieval kernels (see Ref. [S21] and Sec. 6.4 below).

We consider the so-called adiabatic EIT storage [S21] where a single-photon wave packet is incident on the ensemble and is mapped onto a spin wave. Using the state labels in Fig. 1(a) and Fig. 1(b) of the main article, a spin wave is a superposition of states where a single atom is in state $|c\rangle$ and the rest are in state $|a\rangle$. We assume a constant Rabi frequency of the classical drive $\Omega(z) = \Omega_0$, but choosing a co-propagating classical drive with Rabi frequency

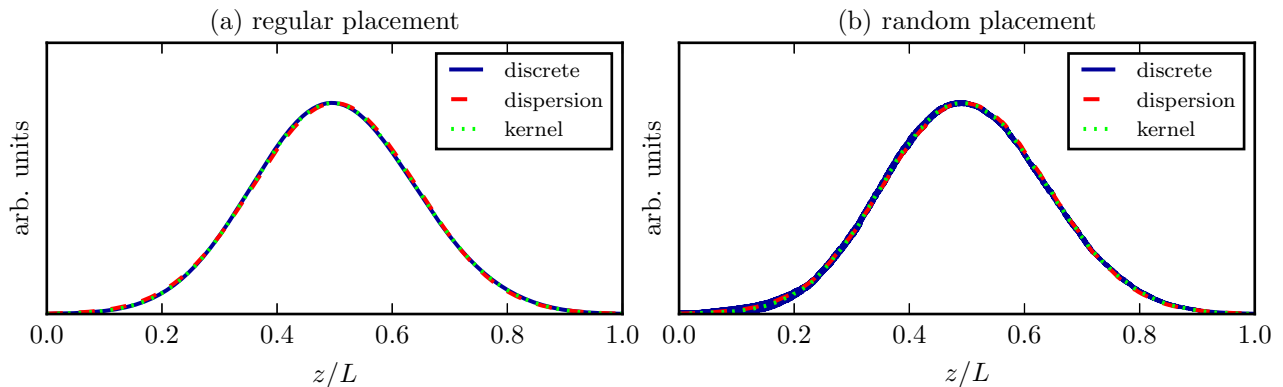


FIG. S9. The stored Gaussian spin wave computed using three different models for EIT storage: the dispersion relation of Sec. 6.2 (“dispersion”), the fully discrete theory of Sec. 6.3 (“discrete”), and the storage kernel of Sec. 6.4 (“kernel”). Contrary to the fidelity calculations, the field is incident from one side (left) only to show the influence of random placement of the atoms more clearly. The common parameters for the two subplots are $\Gamma_{1D}/\Gamma = 0.05$, $N = 10^4$, $\Omega_0/\Gamma = 1$, $\sigma/L = 0.1$ (width of the stored Gaussian spin wave). (a) Regularly placed atoms are assumed with inter-atomic distance $d = 0.266\pi/k_0$. All three curves are nearly indistinguishable from each other. (b) Randomly placed atoms where the position of each atom is chosen from a uniform distribution over the whole ensemble. The average density is the same as in (a). The curve for the fully discrete storage differs slightly from the two others and exhibits rapid variation with position that appears as if the line itself is thicker. This rapid variation becomes more visible for higher values of Γ_{1D}/Γ .

$\Omega(z) = \Omega_0 e^{\pm ik_0 z}$ will only change the spatially-dependent phase factor of the stored spin wave. In the limit of high storage efficiency, the temporal profile of the photon and the spatial profile of the stored spin wave will approximately have the same form. E.g. if a photon with Gaussian temporal wave packet is stored, the resulting spin wave will have a Gaussian spatial profile. This is a consequence of the time-independent Rabi frequency of the classical drive, and it allows us to use the EIT dispersion relation to describe the storage and retrieval.

The EIT dispersion relation is used to gain intuition about the storage and retrieval process and also for the analytical calculations. In the numerical calculations of the fidelities and success probability, the atoms are always modeled as being discrete. However, the fully discrete EIT storage and retrieval model (Sec. 6.3) becomes very computationally demanding as the number of atoms increases. Therefore, to be able to calculate fidelities with a large number of atoms, we instead use the less computationally demanding storage and retrieval kernels derived using the continuum model of the atomic ensemble and suitably discretized (Sec. 6.4). In Fig. S9(a), we show that the three models agree very well for the case of regularly placed atoms with large optical depth $d_{\text{opt}} = 2N\Gamma_{1D}/\Gamma = 1000$. For randomly placed atoms in Fig. S9(b), the fully discrete theory gives slightly different results compared to using the discretized continuum theories (dispersion relation or storage kernel). If Γ_{1D}/Γ is increased, there are more significant differences that we believe to be caused by the continuum theory not accounting for the reflection of parts of the propagating excitation due to disorder. Since we consider a relatively small $\Gamma_{1D}/\Gamma = 0.05$ in most of our numerical examples, we always use the discretized continuum kernels for storage and retrieval, even for randomly placed atoms (in Fig. S15 below).

6.2. Using the dispersion relation

The adiabatic EIT storage and retrieval can be modeled in a particularly simple way if the influence of the interface between the atomic medium and vacuum is ignored. To use the EIT dispersion relation, we need to assume that the ensemble is of infinite extent. However, to compute the storage and retrieval efficiency, we need to assume propagation through a finite ensemble. In the calculations below, this is reflected in infinite bounds for the integration but a finite propagation length. The only processes that happen in this model is that the stored photon wave packet broadens in space as it propagates, and its norm decays due to spontaneous emission. The EIT storage and retrieval efficiency will then be the norm of the wave packet that has propagated for the full length of the ensemble L (with a stop at $L/2$ to allow for the second photon to be scattered off the ensemble).

The EIT dispersion relation is [S19]

$$\delta_k \approx v_g(k - k_0) + \frac{1}{2}\alpha(k - k_0)^2 \quad (\text{S99})$$

with

$$v_g = \frac{2L|\Omega_0|^2}{N\Gamma_{1D}}, \quad \alpha = -i\frac{4L^2|\Omega_0|^2\Gamma'}{N^2\Gamma_{1D}^2}. \quad (\text{S100})$$

In rescaled coordinates $\tilde{z} = z/L$ and wave vectors $\tilde{k} = kL$ the dispersion relation can be written

$$\delta_{\tilde{k}} \approx \tilde{v}_g(\tilde{k} - \tilde{k}_0) + \frac{1}{2}\tilde{\alpha}(\tilde{k} - \tilde{k}_0)^2 \quad (\text{S101})$$

with

$$\tilde{v}_g = \frac{v_g}{L} = \frac{2|\Omega_0|^2}{N\Gamma_{1D}}, \quad \tilde{\alpha} = \frac{\alpha}{L^2} = -i\frac{4|\Omega_0|^2\Gamma'}{N^2\Gamma_{1D}^2}. \quad (\text{S102})$$

We only consider incident photons where the temporal profile is Gaussian. When such a photon is mapped onto a stored excitation, this results in an approximately Gaussian spatial profile of the form

$$S(\tilde{z}) = \frac{1}{(2\pi\tilde{\sigma}^2)^{1/4}} \exp\left(-\frac{(\tilde{z} - \tilde{\mu})^2}{4\tilde{\sigma}^2}\right) e^{i\tilde{k}_0\tilde{z}}, \quad (\text{S103})$$

where the rescaled quantities are $\tilde{\sigma} = \sigma/L$, $\tilde{\mu} = \mu/L$, $\tilde{k}_0 = k_0L$. The spatial profile at later times, can be found by Fourier transforming $S(z)$, multiplying the Fourier transform by $\exp(-i\delta_{\tilde{k}}t)$, and taking the inverse Fourier transform. We obtain

$$S(\tilde{z}, t) = \frac{1}{(2\pi\tilde{\sigma}^2)^{1/4}} \sqrt{\frac{1}{1 + i\tilde{\alpha}t/(2\tilde{\sigma}^2)}} \exp\left(-\frac{(\tilde{z} - \tilde{\mu} - \tilde{v}_gt)^2}{4\tilde{\sigma}^2(1 + i\tilde{\alpha}t/(2\tilde{\sigma}^2))}\right) e^{i\tilde{k}_0\tilde{z}}. \quad (\text{S104})$$

The norm squared of the wave packet at a time $t \geq 0$ is given by

$$\mathcal{N}_S^2(t) = \int_{-\infty}^{\infty} |S(\tilde{z}, t)|^2 d\tilde{z} = \frac{1}{\sqrt{1 + i\tilde{\alpha}t/(2\tilde{\sigma}^2)}}. \quad (\text{S105})$$

The combined storage and retrieval efficiency η_{EIT} is given by Eq. (S105) with $t = 1/\tilde{v}_g = L/v_g$, i.e. the time required to pass the whole ensemble. We thereby get

$$\eta_{\text{EIT}} = \mathcal{N}_S^2(t = 1/\tilde{v}_g) = \frac{1}{\sqrt{1 + \frac{\Gamma'}{N\Gamma_{1D}\tilde{\sigma}^2}}} \approx 1 - \frac{1}{2} \frac{\Gamma'}{N\Gamma_{1D}\tilde{\sigma}^2}. \quad (\text{S106})$$

6.3. Using the fully discrete theory

Using the intuition about EIT from Sec. 6.2, we can implement numerical simulations of EIT storage and retrieval accounting for the discrete nature of the atoms. This approach is very similar to the ‘‘electric field elimination’’ approach of Ref. [S20]. The main difference is that, since storage and retrieval of a single photon only requires calculating the dynamics in the atomic single-excitation manifold, we can eliminate the electric field directly in the Schrödinger picture instead of the Heisenberg picture in Ref. [S20].

The electric field operator can be written $\hat{\mathcal{E}}(z) = \hat{\mathcal{E}}_+(z)e^{ik_0z} + \hat{\mathcal{E}}_-(z)e^{-ik_0z}$, where $\hat{\mathcal{E}}_+$ and $\hat{\mathcal{E}}_-$ are the parts of the field that propagate to the right (positive direction) and left (negative direction), respectively. The two parts are assumed to be completely separate fields, and their commutators are

$$[\hat{\mathcal{E}}_\alpha(z), \hat{\mathcal{E}}_\beta^\dagger(z')] = \delta_{\alpha\beta}\delta(z - z'), \quad (\text{S107})$$

where $\alpha, \beta \in \{+, -\}$.

The Hamiltonian for the ensemble of Λ -type atoms coupled to the electric field is $\hat{H} = \hat{H}_a + \hat{H}_i + \hat{H}_p$, representing the atomic, interaction and photonic Hamiltonian, respectively. The three parts of the Hamiltonian are given by

$$\hat{H}_a = -\hbar \sum_j \left[\left(\Delta_0 + i \frac{\Gamma'}{2} \right) \hat{\sigma}_{bb,j} + \delta_0 \hat{\sigma}_{cc,j} \right], \quad (\text{S108})$$

$$\hat{H}_i = -\hbar \sum_j \left\{ [\hat{\sigma}_{bc,j} \Omega_0 + \text{H.c.}] + g \sqrt{2\pi} [\hat{\sigma}_{ba,j} \hat{\mathcal{E}}(z_j) + \text{H.c.}] \right\}, \quad (\text{S109})$$

$$\hat{H}_p = -i\hbar c \int \left[\hat{\mathcal{E}}_+^\dagger(z) \frac{\partial \hat{\mathcal{E}}_+(z)}{\partial z} - \hat{\mathcal{E}}_-^\dagger(z) \frac{\partial \hat{\mathcal{E}}_-(z)}{\partial z} \right] dz, \quad (\text{S110})$$

where c is the speed of light (group velocity in the waveguide). We assume that the detuning Δ_0 is always set to zero during storage and retrieval (this was also assumed in Sec. 6.2 above). However, if desired, off-resonant ($\Delta_0 \neq 0$) EIT storage and retrieval is also possible [S21], and hence we keep the Δ_0 term in the equations of motion below for completeness.

In the single-excitation manifold, the state can be written

$$|\psi(t)\rangle = \sum_j (P_j(t) \hat{\sigma}_{ba,j} + S_j(t) \hat{\sigma}_{ca,j}) |a\rangle^N |\text{vac}\rangle + \left(\int \frac{\Phi_+(z,t)}{\sqrt{c}} \hat{\mathcal{E}}_+^\dagger(z) |\text{vac}\rangle dz + \int \frac{\Phi_-(z,t)}{\sqrt{c}} \hat{\mathcal{E}}_-^\dagger(z) |\text{vac}\rangle dz \right) |a\rangle^N. \quad (\text{S111})$$

From the Schrödinger equation, we get the equations of motion for the atomic coefficients

$$\frac{\partial P_j}{\partial t} = \left(i\Delta_0 - \frac{\Gamma'}{2} \right) P_j + i\Omega_0 S_j + i\sqrt{\frac{\Gamma_{1D}}{2}} \left(\Phi_+(z_j, t) e^{ik_0 z_j} + \Phi_-(z_j, t) e^{-ik_0 z_j} \right), \quad (\text{S112})$$

$$\frac{\partial S_j}{\partial t} = i\delta_0 S_j + i\Omega_0^* P_j, \quad (\text{S113})$$

where $\Gamma_{1D} = 4\pi g^2/c$. For the electric field coefficients Φ_\pm , we have the equations

$$\left(\frac{\partial}{\partial t} \pm c \frac{\partial}{\partial z} \right) \Phi_\pm(z, t) = ic \sqrt{\frac{\Gamma_{1D}}{2}} \sum_j \delta(z - z_j) P_j e^{\mp ik_0 z_j}. \quad (\text{S114})$$

These equations can be formally integrated, resulting in

$$\Phi_\pm(z, t) = \Phi_{\pm, \text{in}}(z \mp ct) + i\sqrt{\frac{\Gamma_{1D}}{2}} \sum_j \theta(\pm(z - z_j)) P_j \left(t \mp \frac{z - z_j}{c} \right) e^{\mp ik_0 z_j}, \quad (\text{S115})$$

where $\Phi_{\pm, \text{in}}(z \pm ct)$ are the input fields, and θ is the Heaviside theta function. Inserting these solutions into Eq. (S112) and approximating $P_j(t - |z - z_j|/c) \approx P_j(t)$ [S20], gives

$$\frac{\partial P_j}{\partial t} = \left(i\Delta_0 - \frac{\Gamma'}{2} \right) P_j + i\Omega_0 S_j - \frac{\Gamma_{1D}}{2} \sum_{j'} P_{j'} e^{ik_0 |z_j - z_{j'}|} + i\sqrt{\frac{\Gamma_{1D}}{2}} \left(\Phi_{+, \text{in}}(z_j - ct) e^{ik_0 z_j} + \Phi_{-, \text{in}}(z_j + ct) e^{-ik_0 z_j} \right). \quad (\text{S116})$$

The fidelity calculations in Sec. 3 above are formulated in terms of $\phi_{A, \text{in}}(t)$ and $\phi_{A, \text{out}}(t)$ that are the input field to be stored and the retrieved output field, respectively. (There are two different output fields, $\phi_{A, \text{out}, 0}(t)$ and $\phi_{A, \text{out}, 1}(t)$, but for the discussion of storage and retrieval, the difference between them is not important.) We need to account for the beam splitter in the Sagnac interferometer. Hence, the relations between the fields in this section and Sec. 3 are

$$\Phi_{+, \text{in}}(z_j - ct) = \frac{1}{\sqrt{2}} \phi_{A, \text{in}}(t - z_j/c), \quad (\text{S117})$$

$$\Phi_{-, \text{in}}(z_j + ct) = \frac{1}{\sqrt{2}} \phi_{A, \text{in}}(t - (L - z_j)/c), \quad (\text{S118})$$

$$\phi_{A, \text{out}}(t) = \frac{1}{\sqrt{2}} (\Phi_+(L, t) + \Phi_-(0, t)). \quad (\text{S119})$$

Note that the field is incident from two directions in order to ensure that no excitations are stored on atoms at the nodes of the standing wave of the classical drive applied during the scattering for the Λ -type scheme. The conditions for this may not necessarily be the same as the conditions derived for scattering from the Sagnac interferometer (see Sec. 5). If this is an issue, it can be compensated by adjusting the position of the atoms between storage and scattering, e.g., by adjusting the phases of the trapping lasers or of the classical drives. For the dual-V scheme, there is no phase requirement during storage and this is not a concern.

As the input wave function, we choose

$$\phi_{A,\text{in}}(t) = \frac{1}{(2\pi\sigma_{\text{in}}^2)^{1/4}} \exp\left(-\frac{(t - \mu_{\text{in}})^2}{4\sigma_{\text{in}}^2}\right) \quad (\text{S120})$$

where the width and central time,

$$\sigma_{\text{in}} = \sigma / \left(v_{\text{g}} \sqrt{1 + i\alpha L / (4\sigma^2 v_{\text{g}})} \right), \quad (\text{S121})$$

$$\mu_{\text{in}} = 4\sigma_{\text{in}}, \quad (\text{S122})$$

are defined in terms of the EIT group velocity (S100). The factor $\sqrt{1 + i\alpha L / (4\sigma^2 v_{\text{g}})}$ (a real number, since α is imaginary) in the definition of σ_{in} is introduced to compensate for the spin wave becoming wider as it propagates inside the ensemble (see Eq. (S104)). This particular factor is chosen such that the stored Gaussian spin wave (centered at the position $L/2$) has width σ . In the end, since we optimize over σ , this adjustment has no effect on the final values of the numerically calculated fidelities and success probability. However, it ensures that the optimal σ in the numerical calculations is similar to the optimal value found by neglecting broadening of the spin wave under propagation.

In the fully discrete model, we do not explicitly calculate the storage and retrieval kernels that appear in Eqs. (S27) and (S28). Instead, we calculate the action of these kernels on respectively a specific $\phi_{A,\text{in}}(t)$ or a spin wave given by the coefficients S_j . For storage, this amounts to numerically solving Eqs. (S113) and (S116) for a given $\phi_{A,\text{in}}(t)$ and the initial condition $P_j = S_j = 0$ at $t = 0$. We take the stored spin wave to be the coefficients S_j at $t = \mu_{\text{in}}/c + L/(2v_{\text{g}})$. This final time is the sum of the time for propagation through vacuum and (half of) the EIT medium. For retrieval, Eqs. (S113) and (S116) are solved with $\phi_{A,\text{in}}(t) = 0$ under the initial conditions that at $t = 0$ the coefficients $S_j(t = 0)$ are set to the spin wave that is to be retrieved, and $P_j(t = 0) = 0$. At each time step, we calculate $\phi_{A,\text{out}}(t)$ using Eqs. (S115) with $P_j(t \mp (z - z_j)/c) \approx P_j(t)$ along with Eq. (S119). We assume that the retrieval happens until $t = L/v_{\text{g}}$, i.e. the time that it takes for the EIT polaritons to move through the whole ensemble.

6.4. Using the storage and retrieval kernels

As an approximation to the fully discrete theory of Sec. 6.3, one can use the continuum theory of Ref. [S21]. The continuum approximation allows the derivation of explicit expressions for the linear maps (given in terms of integration with a particular kernel) describing storage and retrieval.

Before doing the continuum approximation, we first rewrite the Hamiltonian (S108) in terms of the collective operators

$$\hat{\sigma}_{\alpha\beta}(z) = \frac{1}{n_0} \sum_j \delta(z - z_j) \hat{\sigma}_{\alpha\beta,j}, \quad (\text{S123})$$

where $\alpha, \beta \in \{a, b, c\}$, and $n_0 = N/L$ is the average density. These collective operators have the equal time commutation relation

$$[\hat{\sigma}_{\alpha\beta}(z), \hat{\sigma}_{\alpha'\beta'}(z')] = \frac{1}{n_0} \delta(z - z') (\delta_{\beta,\alpha'} \hat{\sigma}_{\alpha\beta'} - \delta_{\beta',\alpha} \hat{\sigma}_{\alpha'\beta}). \quad (\text{S124})$$

Using the collective atomic operators, the Hamiltonian (S108) is

$$\hat{H}_a = -\hbar n_0 \int \left[\left(\Delta_0 + i \frac{\Gamma'}{2} \right) \hat{\sigma}_{bb}(z) + \delta_0 \hat{\sigma}_{cc}(z) \right] dz \quad (\text{S125})$$

$$\hat{H}_i = -\hbar n_0 \int \left\{ [\hat{\sigma}_{bc}(z) \Omega_0 + \text{H.c.}] + g \sqrt{2\pi} [\hat{\sigma}_{ba}(z) \hat{\mathcal{E}}(z) + \text{H.c.}] \right\} dz \quad (\text{S126})$$

$$\hat{H}_p = -i\hbar c \int \left[\hat{\mathcal{E}}_+^\dagger(z) \frac{\partial \hat{\mathcal{E}}_+(z)}{\partial z} - \hat{\mathcal{E}}_-^\dagger(z) \frac{\partial \hat{\mathcal{E}}_-(z)}{\partial z} \right] dz. \quad (\text{S127})$$

Instead of the state (S111), we use

$$\begin{aligned} |\psi(t)\rangle = & \int \left(\frac{\sqrt{N}}{L} P(z, t) \hat{\sigma}_{ba}(z) + \frac{\sqrt{N}}{L} S(z, t) \hat{\sigma}_{ca}(z) \right) |a\rangle^N |\text{vac}\rangle dz \\ & + \left(\int \frac{\Phi_+(z, t)}{\sqrt{c}} \hat{\mathcal{E}}_+^\dagger(z) |\text{vac}\rangle dz + \int \frac{\Phi_-(z, t)}{\sqrt{c}} \hat{\mathcal{E}}_-^\dagger(z) |\text{vac}\rangle dz \right) |a\rangle^N. \end{aligned} \quad (\text{S128})$$

Note that if, for example, the excitation is entirely in the metastable states at a time t , we have

$$1 = \langle \psi(t) | \psi(t) \rangle = \frac{N}{L^2} \iint S^*(z, t) S(z', t) [\hat{\sigma}_{ab}(z), \hat{\sigma}_{ba}(z')] dz = \frac{1}{L} \iint |S(z, t)|^2 dz, \quad (\text{S129})$$

where we used the continuum approximation $\sum_j \delta(z - z_j) \approx n_0$ [S11] together with the low excitation approximation $\sigma_{aa,j} \approx 1$ to get $\sigma_{aa}(z) \approx 1$ and $\sigma_{bb} \approx 0$. Equation (S129) also gives the normalization condition for S in the continuum model (and similarly for P).

The equations of motion for the coefficients are

$$\left(\frac{\partial}{\partial t} \pm c \frac{\partial}{\partial z} \right) \Phi_\pm(z, t) = ic \sqrt{\frac{\Gamma_{1D} N}{2}} \frac{1}{L} P(z, t), \quad (\text{S130})$$

$$\frac{\partial}{\partial t} P(z, t) = \left(i\Delta_0 - \frac{\Gamma'}{2} \right) P(z, t) + i\Omega_0 S(z, t) + i \sqrt{\frac{\Gamma_{1D} N}{2}} \left(\Phi_+(z, t) e^{ik_0 z} + \Phi_-(z, t) e^{-ik_0 z} \right), \quad (\text{S131})$$

$$\frac{\partial}{\partial t} S(z, t) = i\delta_0 S(z, t) + i\Omega_0^* P(z, t). \quad (\text{S132})$$

As an extension to the theory of Ref. [S21], we want to consider an input field that can be incident from both sides instead of only one. The approach that we use is to consider the parts of the single photon excitation incident from the opposite sides as being stored separately from each other. When doing this, we ignore the fact that the two parts have opposite spatial phases $e^{\pm ik_0 z}$ that interfere inside the ensemble to produce a spatially modulated spin wave with amplitude proportional to $\cos(k_0 z)$.

Such spatial modulation of the stored spin wave is very important for the Λ -scheme, since the part of the excitation that is stored on the nodes of the standing wave of the classical drive does not significantly change the scattering properties of the ensemble (see Sec. 4.2.2). Expressed in terms of the notation introduced in the fidelity calculations (see Eq. (S28)), we have $R_{1,j}(\delta_B) \approx R_0(\delta_B)$ for odd j with atoms placed at positions $z_j = j\pi/(2k_0)$ (where $0 \leq j \leq N-1$), i.e. $k_0 z_j$ being an odd multiple of $\pi/2$. With the photon incident from both sides, there is no amplitude on these atoms, since $S(z_j) \propto \cos(k_0 z_j) = 0$ for odd j . This is correctly reproduced by the fully discrete model of Sec. 6.3, since it always accounts for the phases of free propagation. On the other hand, due to the removal of the rapidly varying spatial phases in the continuum theory, this factor $\cos(k_0 z_j)$ is not present in the two separate parts of the stored spin wave, incorrectly resulting in non-zero probability of storage into the atoms at positions $z_j = j\pi/(2k_0)$ with odd j . To prevent acquiring a reflection coefficient with a wrong phase ($R_0(\delta_B)$) at these atomic positions, we set $R_{1,j}(\delta_B) = R_{1,j-1}(\delta_B)$ for odd j , effectively redistributing the stored photon such that it is only stored on atoms with even j . As we show in Fig. S10, this phenomenological adjustment of the reflection coefficient in the continuum model gives results that are essentially indistinguishable from the results produced by the fully discrete model of Sec. 6.3. For the dual-V scheme, no such adjustment of the reflection coefficients is needed neither in the continuum nor the discrete model, which also produce indistinguishable results.

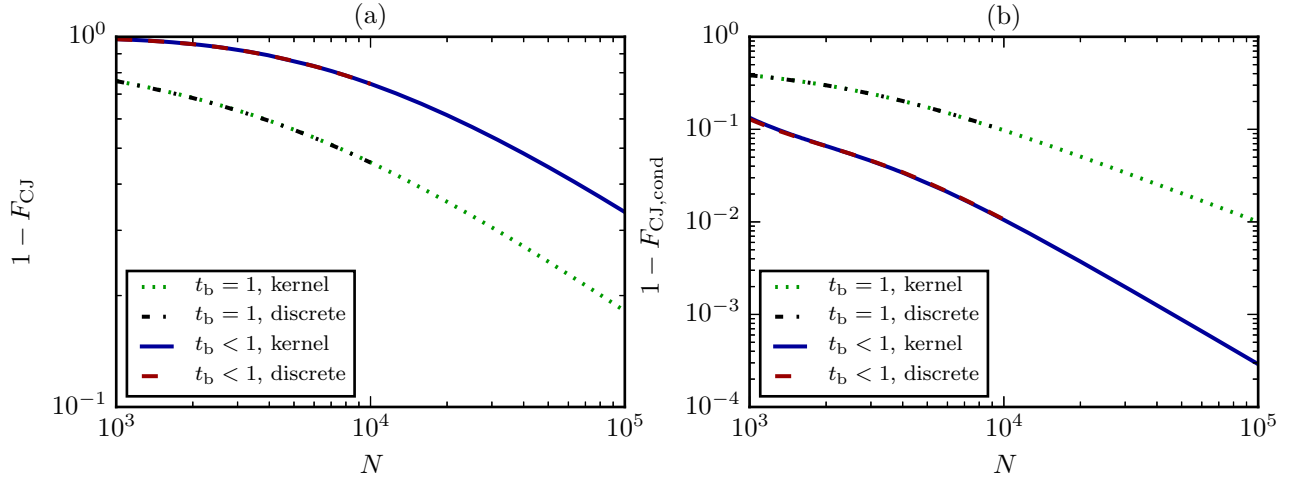


FIG. S10. Comparison of (a) unconditional and (b) conditional Choi-Jamiolkowski fidelities for the Λ -type scheme with different models used for EIT storage and retrieval plotted as functions of the number of atoms N with fixed $\Gamma_{1D}/\Gamma = 0.05$ and $\Omega_0/\Gamma = 1$. Under EIT (storage and retrieval), $\Omega(z) = \Omega_0$. Under stationary light (scattering), $\Omega(z) = \Omega_0 \cos(k_0 z)$. The “discrete” plots use the fully discrete theory of Sec. 6.3, and the “kernel” plots use the discretized continuum storage and retrieval kernels discussed in Sec. 6.4. In both cases, the optimal Δ_c and $\tilde{\sigma}$ (width of the stored Gaussian spin wave) are found by doing numerical optimization using the discretized continuum storage and retrieval kernels, since the fully discrete model is computationally much more demanding.

The fields incident from the left and right couple to different components of the atomic coefficients that can be written

$$P(z, t) = P_+(z, t)e^{ik_0 z} + P_-(z, t)e^{-ik_0 z}, \quad (\text{S133})$$

$$S(z, t) = S_+(z, t)e^{ik_0 z} + S_-(z, t)e^{-ik_0 z}. \quad (\text{S134})$$

After inserting these definitions into Eqs. (S130), (S131) and (S132) and separating the components, we get

$$\left(\frac{\partial}{\partial t} \pm c \frac{\partial}{\partial z}\right) \Phi_{\pm}(z, t) = ic\sqrt{\frac{\Gamma_{1D}N}{2}} \frac{1}{L} P_{\pm}(z, t), \quad (\text{S135})$$

$$\frac{\partial}{\partial t} P_{\pm}(z, t) = \left(i\Delta_0 - \frac{\Gamma'}{2}\right) P_{\pm}(z, t) + i\Omega_0 S_{\pm}(z, t) + i\sqrt{\frac{\Gamma_{1D}N}{2}} \Phi_{\pm}(z, t), \quad (\text{S136})$$

$$\frac{\partial}{\partial t} S_{\pm}(z, t) = i\delta_0 S_{\pm}(z, t) + i\Omega_0^* P_{\pm}(z, t), \quad (\text{S137})$$

To solve for Φ_+ , P_+ and S_+ , the approach in Ref. [S21] can be used directly. It consists of transforming into the coordinates $\tilde{z} = z/L$ and $\tilde{t} = t - z/c$, Laplace transforming in the spatial coordinate \tilde{z} , solving the equations of the Laplace transforms (under the adiabatic approximation $\frac{\partial}{\partial \tilde{t}} P_+ \approx 0$) and taking the inverse Laplace transform. As a minor modification, we also transform back from the co-propagating time coordinate $\tilde{t} = t - z/c$ to the original t (by replacing all \tilde{t} by t in the final expressions). Solving for Φ_- , P_- and S_- is simply a spatial reflection of the original problem around $\tilde{z} = 1/2$. We find that the stored spin wave is

$$S_+(\tilde{z}, t) = \int_0^t K_s(\tilde{z}, t - t') \Phi_+(\tilde{z} = 0, t') dt', \quad (\text{S138})$$

$$S_-(\tilde{z}, t) = \int_0^t K_s(1 - \tilde{z}, t - t') \Phi_-(\tilde{z} = 1, t') dt', \quad (\text{S139})$$

where the storage kernel (in the adiabatic approximation) is

$$K_s(\tilde{z}, t) \approx -\frac{\sqrt{b}\Omega_0^* e^{i\delta_0 t}}{(\Gamma'/2) - i\Delta_0} I_0\left(2\frac{\sqrt{|\Omega_0|^2 t b \tilde{z}}}{(\Gamma'/2) - i\Delta_0}\right) \exp\left(-\frac{|\Omega_0|^2 t + b\tilde{z}}{(\Gamma'/2) - i\Delta_0}\right), \quad (\text{S140})$$

written in terms of $b = (N\Gamma_{1D})/2$ (related to the resonant optical depth by $d_{\text{opt}} = 4b/\Gamma$) and the modified Bessel function of the first kind I_0 . The retrieved field is

$$\Phi_+(\tilde{z} = 1, t) = \int_0^1 K_r(\tilde{z}, t) S_+(\tilde{z}, t = 0) d\tilde{z}, \quad (\text{S141})$$

$$\Phi_-(\tilde{z} = 0, t) = \int_0^1 K_r(1 - \tilde{z}, t) S_-(\tilde{z}, t = 0) d\tilde{z}, \quad (\text{S142})$$

where the retrieval kernel is

$$K_r(\tilde{z}, t) \approx -\frac{\sqrt{b}\Omega_0 e^{i\delta_0 t}}{(\Gamma'/2) - i\Delta_0} I_0\left(2\frac{\sqrt{|\Omega_0|^2 t b(1 - \tilde{z})}}{(\Gamma'/2) - i\Delta_0}\right) \exp\left(-\frac{|\Omega_0|^2 t + b(1 - \tilde{z})}{(\Gamma'/2) - i\Delta_0}\right). \quad (\text{S143})$$

The stored spin waves are such that they are centered at $\tilde{z} = 1/2$ and become narrower in space for increasing optical depth (see the fidelity derivations in Sec. 9 below). The input and output photon wave functions are centered around times $t \propto L/v_g = N\Gamma_{1D}/(2|\Omega_0|^2) = b/|\Omega_0|^2$. Inserting these mean values into Eqs. (S140) and (S143), we see that the argument of I_0 becomes very big, since $\sqrt{|\Omega_0|^2 t b \tilde{z}} = \sqrt{|\Omega_0|^2 t b(1 - \tilde{z})} \propto b$ and $\Delta_0 = 0$. This allows us to use the asymptotic expansion $I_0(x) \approx \exp(x)/\sqrt{2\pi x}$ that is valid for $|x| \gg 1$ and $\arg(x) < \pi/2$. In this limit, the kernels become

$$K_s(\tilde{z}, t) \approx -\frac{\sqrt{b}\Omega_0^* e^{i\delta t}}{2\sqrt{\pi}\sqrt{(\Gamma'/2) - i\Delta_0}} \frac{1}{(|\Omega_0|^2 t b \tilde{z})^{1/4}} \exp\left(-\frac{(\sqrt{|\Omega_0|^2 t} - \sqrt{b\tilde{z}})^2}{(\Gamma'/2) - i\Delta_0}\right), \quad (\text{S144})$$

$$K_r(\tilde{z}, t) \approx -\frac{\sqrt{b}\Omega_0 e^{i\delta t}}{2\sqrt{\pi}\sqrt{(\Gamma'/2) - i\Delta_0}} \frac{1}{(|\Omega_0|^2 t b(1 - \tilde{z}))^{1/4}} \exp\left(-\frac{(\sqrt{|\Omega_0|^2 t} - \sqrt{b(1 - \tilde{z})})^2}{(\Gamma'/2) - i\Delta_0}\right). \quad (\text{S145})$$

These formulas have a better numerical behavior compared to Eqs. (S140) and (S143), since one does not need to multiply the value of the I_0 (exponentially large) with an exponentially small factor. Hence, we always use Eqs. (S144) and (S145) in the numerical calculations.

The relations between the fields in this section and Sec. 3 are

$$\Phi_+(\tilde{z} = 0, t) = \frac{1}{\sqrt{2}} \phi_{A,\text{in}}(t), \quad (\text{S146})$$

$$\Phi_-(\tilde{z} = 1, t) = \frac{1}{\sqrt{2}} \phi_{A,\text{in}}(t), \quad (\text{S147})$$

$$\phi_{A,\text{out}}(t) = \frac{1}{\sqrt{2}} (\Phi_+(\tilde{z} = 1, t) + \Phi_-(\tilde{z} = 0, t)), \quad (\text{S148})$$

where $\phi_{A,\text{in}}(t)$ is given by Eq. (S120) like in the fully discrete model.

The results of this section assume that the atoms can be modeled as a continuum, but the scattering coefficients in Eq. (S28) are only given at the discrete atom positions. Hence, we need to sample the resulting continuum solutions at the discrete positions of the atoms. In the numerical calculations, the continuum solutions are always sampled as if the atoms were placed regularly independent of the actual placement. To justify regular sampling, we note that instead of the rescaled position coordinate $\tilde{z} = z/L$, one could use $\tilde{z} = \int_0^z (n_0(z')/N) dz'$ [S21], where $n_0(z)$ is the local density of the atoms. For an average density $n_0 = N/L$, this rescaled coordinate is equivalent to $\tilde{z} = z/L$. For the local density $n_0(z) = \sum_j \delta(z - z_j)$, the rescaled position becomes $\tilde{z} = \sum_j \theta(z - z_j)/N$, where θ is the Heaviside theta function. With the convention $\theta(0) = 0$, each z_j (where $0 \leq j \leq N - 1$) is transformed into $\tilde{z} = j/N$ regardless of the actual value of z_j .

Having in mind both the separation of the spin waves into two independent parts and the sampling of the continuum solutions at regular intervals, we can define the storage and retrieval kernels that will be used in Eqs. (S27) and (S28). We define the vector representing the spin wave to have $2N$ elements—for two separately stored spin waves that have fields incident either from the left or from the right as the input. Using the same storage time $\mu_{\text{in}}/c + L/(2v_g)$ as for the discrete model in Sec. 6.3, the storage kernel is

$$K_{s,j}(t_A) = K_s(\tilde{z} = j/N, t = \mu_{\text{in}}/c + L/(2v_g) - t_A) / \sqrt{N} \text{ for } 0 \leq j \leq N - 1, \quad (\text{S149})$$

$$K_{s,j}(t_A) = K_s(\tilde{z} = 1 - (j - N)/N, t = \mu_{\text{in}}/c + L/(2v_g) - t_A) / \sqrt{N} \text{ for } N \leq j \leq 2N - 1, \quad (\text{S150})$$

where we have assumed that the coefficients corresponding to S_+ are stored in the part of the vector with indices $0 \leq j \leq N-1$, and the coefficients corresponding to S_- are stored in the part of the vector with $N \leq j \leq 2N-1$. The retrieval kernel is

$$K_{r,j}(t_A) = K_r(\tilde{z} = j/N, t = t_A)/\sqrt{N} \text{ for } 0 \leq j \leq N-1, \quad (\text{S151})$$

$$K_{r,j}(t_A) = K_r(\tilde{z} = 1 - (j-N)/N, t = t_A)/\sqrt{N} \text{ for } N \leq j \leq 2N-1. \quad (\text{S152})$$

As a consequence of having a spin wave vector with $2N$ elements, in Eq. (S28) we define $R_{1,j}(\delta_B) = R_{1,j-N}(\delta_B)$ for $N \leq j \leq 2N-1$.

7. DEPHASING AND DECAY OF THE STORED PHOTON

Depending on the chosen implementation, the classical drive that creates the stationary light (involving states $|a\rangle$, $|b\rangle$ and $|c\rangle$) may also couple state $|d\rangle$ to some excited state. E.g. in the implementation shown in Fig. S5, the classical drive couples state $|d\rangle$ ($F=2$, $m_F=-1$) to state $|f\rangle$ ($F'=2$, $m_{F'}=0$) with a large detuning Δ_{hfs} approximately equal to the hyperfine splitting. This coupling induces both dephasing (when the excitation in state $|f\rangle$ incoherently decays back to state $|d\rangle$) and decay (when the excitation in state $|f\rangle$ incoherently decays to any other possible state).

All the states that $|f\rangle$ can decay into besides $|d\rangle$ can be treated as a single state $|g\rangle$ in a simplified model. In the implementation of Fig. S5, state $|f\rangle$ can also decay to state $|c\rangle$, but we ignore this in this simplified model for two reasons. First, if the π -pulse is perfect, the incoherent part in state $|c\rangle$ will get transferred to state $|d\rangle$ from which any retrieval is suppressed by the large detuning $\sim \Delta_{\text{hfs}}$ of the classical drive. Second, even if the π -pulse is imperfect, the remaining incoherent part in state $|c\rangle$ will have a very low retrieval efficiency due to mode mismatch (see the discussion below).

The Hamiltonian describing coupling of the classical drive to the $|d\rangle \leftrightarrow |f\rangle$ transition is

$$\hat{H}_d = -\hbar \sum_j [\Delta_{\text{hfs}} \hat{\sigma}_{ff,j} + \hat{\sigma}_{fd,j} \Omega_0 + \hat{\sigma}_{df,j} \Omega_0^*]. \quad (\text{S153})$$

The incoherent decay from state $|f\rangle$ is described by the operators

$$\hat{L}_{1,j} = \sqrt{\Gamma_1} \hat{\sigma}_{gf,j}, \quad (\text{S154})$$

$$\hat{L}_{2,j} = \sqrt{\Gamma_2} \hat{\sigma}_{df,j}, \quad (\text{S155})$$

where we assume that $\Gamma' = \Gamma_1 + \Gamma_2$. The evolution of the density matrix ρ is given by the master equation

$$\dot{\rho} = -\frac{i}{\hbar} [H, \rho] - \frac{1}{2} \sum_j \sum_{k=1}^2 \left(\hat{L}_{k,j}^\dagger \hat{L}_{k,j} \rho + \rho \hat{L}_{k,j}^\dagger \hat{L}_{k,j} - 2 \hat{L}_{k,j} \rho \hat{L}_{k,j}^\dagger \right). \quad (\text{S156})$$

If we adiabatically eliminate [S22] the excited state $|f\rangle$, the effective Hamiltonian and decay operators are instead

$$\hat{H}_{d,\text{eff}} = \sum_j \frac{\Delta_{\text{hfs}} |\Omega_0|^2}{\Delta_{\text{hfs}}^2 + \Gamma'^2/4} \hat{\sigma}_{dd,j}, \quad (\text{S157})$$

$$\hat{L}_{1,j,\text{eff}} = \frac{\sqrt{\Gamma_2} \Omega_0}{\Delta_{\text{hfs}} + i\Gamma'/2} \hat{\sigma}_{gd,j}, \quad (\text{S158})$$

$$\hat{L}_{2,j,\text{eff}} = \frac{\sqrt{\Gamma_1} \Omega_0}{\Delta_{\text{hfs}} + i\Gamma'/2} \hat{\sigma}_{dd,j}. \quad (\text{S159})$$

The effective dynamics is then given by

$$\begin{aligned} \dot{\rho} = & -\frac{i}{\hbar} [H_{d,\text{eff}}, \rho] - \frac{\Gamma_{1,\text{eff}}}{2} \sum_j \left(\hat{\sigma}_{dg,j} \hat{\sigma}_{gd,j} \rho + \rho \hat{\sigma}_{dg,j} \hat{\sigma}_{gd,j} - 2 \hat{\sigma}_{gd,j} \rho \hat{\sigma}_{dg,j} \right) \\ & - \frac{\Gamma_{2,\text{eff}}}{2} \sum_j \left(\hat{\sigma}_{dd,j} \hat{\sigma}_{dd,j} \rho + \rho \hat{\sigma}_{dd,j} \hat{\sigma}_{dd,j} - 2 \hat{\sigma}_{dd,j} \rho \hat{\sigma}_{dd,j} \right), \end{aligned} \quad (\text{S160})$$

where

$$\Gamma_{1,\text{eff}} = \frac{\Gamma_1 |\Omega_0|^2}{\Delta_{\text{hfs}}^2 + \Gamma'^2/4}, \quad (\text{S161})$$

$$\Gamma_{2,\text{eff}} = \frac{\Gamma_2 |\Omega_0|^2}{\Delta_{\text{hfs}}^2 + \Gamma'^2/4}. \quad (\text{S162})$$

In general, $\Gamma_{1,\text{eff}}$ and $\Gamma_{2,\text{eff}}$ are respectively set by the T_1 and T_2 times of the system, and Eqs. (S161) and (S162) describe the classical drive induced contributions to these decoherence processes.

We note that dephasing ($\Gamma_{2,\text{eff}}$) has the same effect as decay ($\Gamma_{1,\text{eff}}$) to a good approximation. This is a consequence of the fact that photon A has to be retrieved at the end of the gate protocol. Dephasing creates an incoherent part of state of the stored photon (a classical mixture of excitations in different atoms) that cannot be retrieved in the same way as the coherent part (a superposition of excitations in different atoms) due to lack of mode matching. This can be understood from the simple model of EIT storage described in Sec. 6.2 above. In particular, letting $\sigma \rightarrow 0$ in Eq. (S106) results in $\eta_{\text{EIT}} \rightarrow 0$. Therefore, the retrieved state of an excitation that has experienced dephasing during storage in the ensemble is not different from the state that has experienced decay.

Thus, even if, in principle, dephasing is much worse than population decay for the stored photon (since it cannot be postselected by measuring photon number), the retrieval of the incoherent part of the state is strongly suppressed. Hence, both decay and dephasing can be taken to only affect the unconditional fidelity and success probability and not the conditional fidelity. A more precise analysis of this error on the conditional fidelity may be needed for conditional fidelities that are very close to unity, but we will only limit ourselves to estimating the effect on the unconditional fidelity and success probability. In Sec. 9 below, we show that scattering time t_s (inverse of the bandwidth σ_B) cannot be smaller than approximately $(\Gamma_{1\text{D}}^{3/2} N^{7/4}) / (4\pi^{3/2} \sqrt{\Gamma'} |\Omega_0|^2)$ if high unconditional fidelity and success probability is to be maintained. Hence, the error for the unconditional fidelity and success probability is

$$(\Gamma_{1,\text{eff}} + \Gamma_{2,\text{eff}}) t_s \sim \frac{\Gamma_{1\text{D}}^{3/2} \sqrt{\Gamma'} N^{7/4}}{4\pi^{3/2} \Delta_{\text{hfs}}^2}. \quad (\text{S163})$$

For $\Delta_{\text{hfs}}/\Gamma \sim 10^3$, as in e.g. ^{87}Rb [S6], and choosing $\Gamma_{1\text{D}}/\Gamma = 0.05$, we get the error $\Gamma_{\text{eff}} t_s \sim 5 \cdot 10^{-10} \cdot N^{7/4}$ that is negligible for $N = 10^4$ ($\Gamma_{\text{eff}} t_s \sim 0.005$), but becomes significant for $N = 10^5$ ($\Gamma_{\text{eff}} t_s \sim 0.28$).

8. π -PULSES

Here, we discuss the π -pulses used to reversibly map states $|c\rangle$ and $|d\rangle$. In the implementation of Fig. S5, microwave pulses are assumed, but the mapping could, in principle, also be done with optical fields. The selection of particular m_F -levels is possible due to their splitting in energy by an applied magnetic field. Since the frequency splitting between the adjacent m_F -levels is $\sim \Delta_c$, this determines the time $t_\pi \gtrsim 1/\Delta_c$ needed for a π -pulse.

A possible imperfection in the controlled-phase gate can be caused by a wrong pulse area of the microwave pulse. To model this, we use the Hamiltonian

$$\hat{H}_{\text{mw}} = -\hbar \sum_j \left[\hat{\sigma}_{dc,j} |\Omega_{\text{mw}}\rangle e^{i\phi_{\text{mw}}} + \hat{\sigma}_{cd,j} |\Omega_{\text{mw}}\rangle e^{-i\phi_{\text{mw}}} \right]. \quad (\text{S164})$$

A perfect π -pulse happens when $|\Omega_{\text{mw}}|t = \pi/2$. We parametrize the deviation from a perfect π -pulse by an angle φ and set $|\Omega_{\text{mw}}|t = \pi/2 + \varphi$. To account for a possible deviation from a perfect π -pulse in the fidelity calculations, the analysis in Sec. 3 needs to be extended with assumptions about the evolution of states $|c_j a\rangle$ during scattering. For the computational basis states $|00\rangle$, $|01\rangle$, $|10\rangle$, there is no incident photon B on the atomic ensemble where a part of photon A is stored in the states $|c_j a\rangle$ due to a failed π -pulse. In this case, the evolution of photon A and photon B happens completely separately during scattering. The output wave packet for the part of photon A that was not transferred by both π -pulses can be written

$$\phi_{A,\text{out},a}(t_A) = \sum_{j,j'} \int K_{r,j}(t_A) K_{a,j,j'} K_{s,j'}(t'_A) \phi_{A,\text{in}}(t'_A) dt'_A, \quad (\text{S165})$$

where the kernel $K_{a,j,j'}$ describes the evolution of the states $|c_j a\rangle$ during scattering of photon B . For state $|11\rangle$, the evolution is, in principle, different, because both photons (stationary light polaritons) evolve in the two-excitation

manifold of states (i.e. states like $|c_j c_j' a\rangle = \hat{\sigma}_{ca,j} \hat{\sigma}_{ca,j'} |a\rangle^N$) simultaneously. However, in the limit of few photons and many atoms, stationary light is a linear phenomenon, just like EIT. Thus, we can assume that the two photons evolve separately from each other even for state $|11\rangle$. We thereby arrive at the fidelity in the case of imperfect π -pulses

$$F_{\text{CJ}} = \frac{\eta_{\text{EIT}}}{16} \left| \cos^2(\varphi) \left(2t_b + \int R_0(\delta_B) |\phi_B(\delta_B)|^2 d\delta_B - \frac{1}{\eta_{\text{EIT}}} \iint \phi_{A,\text{out},0}^*(t_A) \phi_{A,\text{out},1}(t_A, \delta_B) |\phi_B(\delta_B)|^2 dt_A d\delta_B \right) + 2 \sin^2(\varphi) \int \phi_{A,\text{out},0}^*(t_A) \phi_{A,\text{out},a}(t_A) dt_A \right|^2. \quad (\text{S166})$$

Note that the factors $\cos(\varphi)$ and $\sin(\varphi)$ appear squared. This reflects the fact that the protocol involves two π -pulses. Hence, a photon is only retrieved if either both π -pulses succeed ($\cos^2(\varphi)$) or fail ($\sin^2(\varphi)$).

The term proportional to $\sin^2(\varphi)$ in Eq. (S166) corresponds to the unwanted process that could degrade the conditional fidelity. Since both π -pulses need to go wrong, it only enters to a higher order, however. The wave packet $\phi_{A,\text{out},a}(t_A)$ in this term could be calculated exactly with the fully discrete theory in Sec. 6.3 (and using $\Omega(z) = \Omega_0 \cos(k_0 z)$ instead of $\Omega(z) = \Omega_0$). However, we will follow a different approach and assume that the excitation in states $|c_j a\rangle$ is simply lost during scattering. This will, to a large extent, happen automatically due evolution of the excitation in states $|c_j a\rangle$ under the conditions of stationary light that has a much higher dissipation rate compared to EIT. If this is not sufficient, an additional EIT retrieval sequence could be done before the second π -pulse to completely remove the part of the excitation still remaining in states $|c_j a\rangle$. Mathematically, this results in $\phi_{A,\text{out},a}(t_A) = 0$, so that the term proportional to $\sin^2(\varphi)$ in Eq. (S166) vanishes.

Thus, the only difference between Eq. (S166) and Eq. (S29) is the overall factor $\cos^4(\varphi)$. This factor merely reflects that an excitation is lost if it was not successfully transferred by both π -pulses. Hence, the same overall factor appears in the success probability P_{suc} , and the conditional fidelity $F_{\text{CJ,cond}} = F_{\text{CJ}}/P_{\text{suc}}$ is unaffected by a wrong pulse area of the microwave pulse.

9. ANALYTICAL FIDELITY OF THE Λ -TYPE SCHEME

Here, we derive

- Eqs. (7)–(10) of the main article.
- The error terms due to imperfectly balanced Sagnac interferrometers.
- The bandwidth dependent correction to Eq. (7) of the main article that is used in the discussion of the gate time.

From Eqs. (1)–(4) of the main article (including the Ω_0 dependent terms, as shown in Eqs. (S67), (S68), (S80) and (S81)) and Eqs. (S96) and (S96) above (assuming $r_{0+} = r_{0-} = r_0$, $t_{0+} = t_{0-} = t_0$, $r_{1+} = r_{1-} = r_1$, $t_{1+} = t_{1-} = t_1$), we find the approximate reflection coefficients of the combined system of the atomic ensemble and the Sagnac

interferometer. They are

$$R_0 = -\frac{1}{2} \left(r_0 \left(e^{2ik_0l_1} + e^{2ik_0l_2} \right) - 2t_0 e^{ik_0(l_1+l_2)} \right) \approx -\frac{1}{2} \left(\left(\frac{\Gamma_{1D}\Gamma'N}{16\Delta_c^2} + \frac{\pi^2\Gamma'|\Omega_0|^2}{2\Delta_c^2\Gamma_{1D}N} \right) \left(e^{2ik_0l_1} + e^{2ik_0l_2} \right) - 2 \left(1 - \frac{\Gamma_{1D}\Gamma'N}{16\Delta_c^2} - \frac{\pi^2\Gamma'|\Omega_0|^2}{2\Delta_c^2\Gamma_{1D}N} \right) e^{ik_0(l_1+l_2)} \right), \quad (\text{S167})$$

$$R_{1,s}(\tilde{z}) = \frac{1}{2} (R_1(\tilde{z}) + R_1(1 - \tilde{z})) = -\frac{1}{4} \left((r_1(\tilde{z}) + r_1(1 - \tilde{z})) \left(e^{2ik_0l_1} + e^{2ik_0l_2} \right) - 2 (t_1(\tilde{z}) + t_1(1 - \tilde{z})) e^{ik_0(l_1+l_2)} \right) \approx -\frac{1}{2} \left(\left(1 - \frac{4\pi^2\Delta_c^2\Gamma'}{\Gamma_{1D}^3N^2} + \frac{32\pi^4\Delta_c^2\Gamma'|\Omega_0|^2}{\Gamma_{1D}^5N^4} - \frac{4\pi^4\Delta_c^2(2\Gamma_{1D} + \Gamma')}{\Gamma_{1D}^3N^2} \left(\tilde{z} - \frac{1}{2} \right)^2 \right) \left(e^{2ik_0l_1} + e^{2ik_0l_2} \right) - 2 \left(\frac{4\pi^2\Delta_c^2\Gamma'}{\Gamma_{1D}^3N^2} - \frac{32\pi^4\Delta_c^2\Gamma'|\Omega_0|^2}{\Gamma_{1D}^5N^4} + \frac{4\pi^4\Delta_c^2\Gamma'}{\Gamma_{1D}^3N^2} \left(\tilde{z} - \frac{1}{2} \right)^2 \right) e^{ik_0(l_1+l_2)} \right). \quad (\text{S168})$$

Note that in the symmetrized reflection coefficient $R_{1,s}(\tilde{z})$, the linear terms proportional to $\pm(\tilde{z} - 1/2)$ (which are present in Eqs. (3) and (4) of the main article) cancel each other. Using the expression for the Gaussian spin wave given by Eq. (S103) with $\tilde{\mu} = 1/2$ we get

$$R_{1,1} \approx \int R_{1,s}(\tilde{z}) |S(\tilde{z})|^2 d\tilde{z} \approx -\frac{1}{2} \left(\left(1 - \frac{4\pi^2\Delta_c^2\Gamma'}{\Gamma_{1D}^3N^2} + \frac{32\pi^4\Delta_c^2\Gamma'|\Omega_0|^2}{\Gamma_{1D}^5N^4} - \frac{4\pi^4\Delta_c^2(2\Gamma_{1D} + \Gamma')}{\Gamma_{1D}^3N^2} \tilde{\sigma}^2 \right) \left(e^{2ik_0l_1} + e^{2ik_0l_2} \right) - 2 \left(\frac{4\pi^2\Delta_c^2\Gamma'}{\Gamma_{1D}^3N^2} - \frac{32\pi^4\Delta_c^2\Gamma'|\Omega_0|^2}{\Gamma_{1D}^5N^4} + \frac{4\pi^4\Delta_c^2\Gamma'}{\Gamma_{1D}^3N^2} \tilde{\sigma}^2 \right) e^{ik_0(l_1+l_2)} \right). \quad (\text{S169})$$

Note that by using Eq. (S103) instead of Eq. (S104) with $t = L/(2v_g)$, it may seem that we have neglected broadening of the spin wave during storage (propagation through the EIT medium for the length $L/2$). However, the definition of σ is taken to be the width of the spin wave after storage, and we make the same choice for the numerical calculations (see the discussion below the Eqs. (S121) and (S122)). The dissipation (decreasing of the norm of Eq. (S104) given by Eq. (S105)) is accounted for separately by the factors η_{EIT} in Eq. (5) of the main article (or Eq. (S29)). Additionally, approximating $R_{1,1} = (1/\eta_{\text{EIT}}) \int \phi_{A,\text{out},0}^*(t) \phi_{A,\text{out},1}(t) dt$ by $R_{1,1} \approx \int R_{1,s}(\tilde{z}) |S(\tilde{z})|^2 d\tilde{z}$ neglects broadening and distortion of the pulse during retrieval. This approximation is valid, since the retrieved wave packet of photon A is expected to be changed in the same way by these effects, regardless of whether photon B was scattered off the ensemble between storage and retrieval or not. This assumption (and all the others required to derive the analytical expressions) is ultimately verified by Fig. S13 below.

To find the influence of an error in the alignment of the Sagnac interferometer, we set $k_0l_2 = 0$ and expand around $k_0l_1 = 0$. The opposite situation (set $k_0l_1 = 0$ and expand around $k_0l_2 = 0$) yields the same result due to symmetry of the expressions under the exchange of l_1 and l_2 . Using Eq. (5) of the main article, an approximation for the unconditional CJ fidelity is

$$F_{\text{CJ}} \approx 1 - \epsilon_b - \frac{\Gamma_{1D}\Gamma'N}{16\Delta_c^2} - \frac{4\pi^2\Delta_c^2\Gamma'}{\Gamma_{1D}^3N^2} - \frac{\pi^2\Gamma'|\Omega_0|^2}{2\Delta_c^2\Gamma_{1D}N} + \frac{32\pi^4\Delta_c^2\Gamma'|\Omega_0|^2}{\Gamma_{1D}^5N^4} - \frac{4\pi^4\Delta_c^2(\Gamma_{1D} + \Gamma')}{\Gamma_{1D}^3N^2} \tilde{\sigma}^2 - \frac{1}{2} \frac{\Gamma'}{N\Gamma_{1D}} \frac{1}{\tilde{\sigma}^2} + \left(-\frac{1}{2} + \frac{3}{8}\epsilon_b + \frac{5\Gamma_{1D}\Gamma'N}{128\Delta_c^2} + \frac{5\pi^2\Delta_c^2\Gamma'}{2\Gamma_{1D}^3N^2} + \frac{5\pi^2\Gamma'|\Omega_0|^2}{16\Delta_c^2\Gamma_{1D}N} - \frac{20\pi^4\Delta_c^2\Gamma'|\Omega_0|^2}{\Gamma_{1D}^5N^4} + \frac{7\pi^4\Delta_c^2\tilde{\sigma}^2}{2\Gamma_{1D}^2N^2} + \frac{5\pi^4\Delta_c^2\Gamma'\tilde{\sigma}^2}{2\Gamma_{1D}^3N^2} \right) (k_0l_1)^2 \quad (\text{S170})$$

where $\epsilon_b = 1 - t_b$, and all error terms (including ϵ_b and k_0l_1) are assumed to be small. In Fig. S11, we plot numerically and analytically calculated fidelities for the imperfectly balanced Sagnac interferometers.

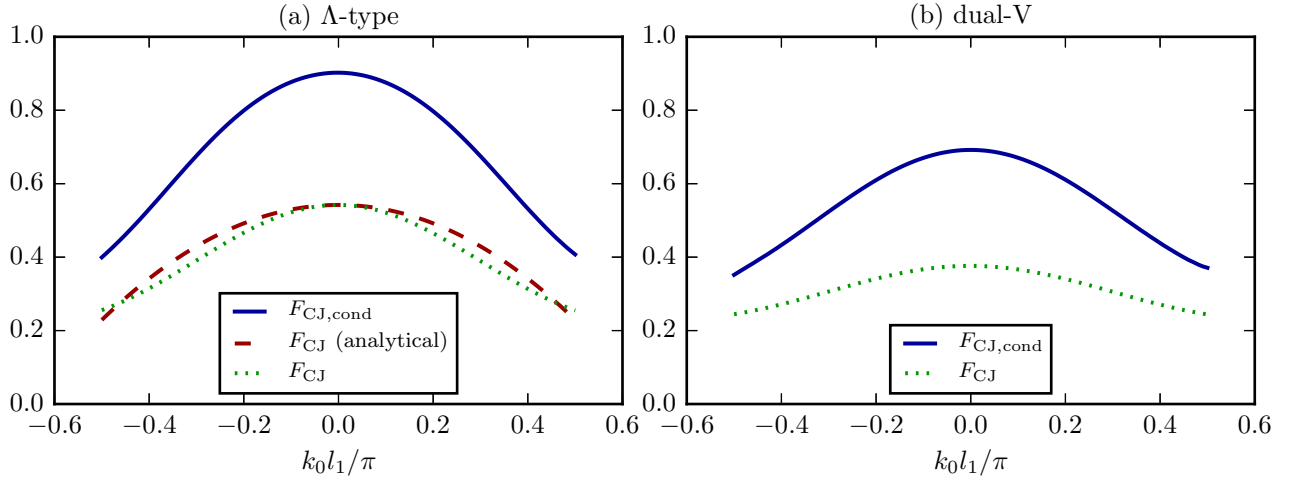


FIG. S11. (a) Unconditional and conditional Choi-Jamiolkowski fidelities for the Λ -type scheme plotted as functions of the length of one of the arms of the Sagnac interferometer l_1 (modulo $2\pi/k_0$), while the other length is held constant $l_2 = 0$ (modulo $2\pi/k_0$) for a fixed number of atoms $N = 10^4$, $\Gamma_{1D}/\Gamma = 0.05$, $\Omega_0/\Gamma = 1$, and interatomic distance $d = 0.5\pi/k_0$. Under EIT (storage and retrieval), $\Omega(z) = \Omega_0$. Under stationary light (scattering), $\Omega(z) = \Omega_0 \cos(k_0 z)$. The fidelities are plotted only for $t_b = 1$. The analytical formula for F_{CJ} is $F_{CJ}(k_0 l_1) = F_{CJ}(0) - (1/2 - (5\pi\Gamma')/(8\Gamma_{1D}\sqrt{N}))(k_0 l_1)^2$. (b) The same but for the dual-V scheme with $d = 0.266\pi/k_0$. Under stationary light (scattering), $\Omega_{\pm}(z) = \Omega_0 e^{\pm i k_0 z}$. For storage and retrieval both in (a) and (b), we use the discretized continuum storage and retrieval kernels discussed in Sec. 6.4.

In principle, if we want to optimize the above expression, we should optimize with respect to Δ_c and $\tilde{\sigma}$ simultaneously (we do this in the numerical calculations). Here, we use an approximate optimization procedure that ignores the fact that some error terms depend on the product of Δ_c and $\tilde{\sigma}$. As we will see, however, these error terms are smaller than the error terms that only depend on Δ_c for fixed Γ_{1D}/Γ and large N . Therefore, we first optimize F_{CJ} over Δ_c separately and then use the optimal value of Δ_c to optimize over $\tilde{\sigma}$. For small $|\Omega_0|$ and $k_0 l_1$, the optimal value of Δ_c is determined by the condition that the third and fourth error terms on the right hand side of Eq. (S170) are equal, i.e.

$$\frac{\Gamma_{1D}\Gamma'N}{16\Delta_c^2} = \frac{4\pi^2\Delta_c^2\Gamma'}{\Gamma_{1D}^3N^2}. \quad (\text{S171})$$

This results in

$$\Delta_c^2 = \frac{\Gamma_{1D}^2 N^{3/2}}{8\pi}. \quad (\text{S172})$$

Inserting this value of Δ_c into Eq. (S170) we obtain

$$F_{CJ} \approx 1 - \epsilon_b - \frac{\pi\Gamma'}{\Gamma_{1D}\sqrt{N}} - \frac{\pi^3(\Gamma_{1D} + \Gamma')}{2\Gamma_{1D}\sqrt{N}}\tilde{\sigma}^2 - \frac{1}{2} \frac{\Gamma'}{N\Gamma_{1D}} \frac{1}{\tilde{\sigma}^2} + \left(-\frac{1}{2} + \frac{3}{8}\epsilon_b + \frac{5\Gamma'\pi}{8\Gamma_{1D}\sqrt{N}} + \frac{\pi^3(7\Gamma_{1D} + 5\Gamma')}{16\Gamma_{1D}\sqrt{N}}\tilde{\sigma}^2 \right) (k_0 l_1)^2. \quad (\text{S173})$$

Note that the Ω_0 dependent terms cancel. In principle, we would need to look at higher order Ω_0 dependent terms to estimate the error from having strong driving (big Rabi frequency Ω_0). For simplicity, however, we restrict ourselves to a numerical investigation. As shown in Fig. S12, even higher order Ω_0 dependent terms can be canceled by adjusting the value of Δ_c . The result is that both the unconditional and conditional fidelities (ignoring the bandwidth of the scattered photon B) are independent of the value of Ω_0 within a wide range. Additionally, Fig. S12 shows that the correction to the optimal Δ_c is negligible for Ω_0 up to 30Γ , so that we can safely use $\Omega_0 = 10\Gamma$ for the discussion of gate time in the main article for the parameters $\Gamma_{1D}/\Gamma = 0.05$ and $N = 10^4$, while keeping Δ_c given by Eq. (S172) that is optimal for weak classical drives. However, if stronger drive fields are available, it should be possible to perform even faster gate operation, provided that there are no other limitations to the strength of the classical drive (e.g. the requirements on frequency separation for the dual-color scheme discussed in Sec. 2 above).

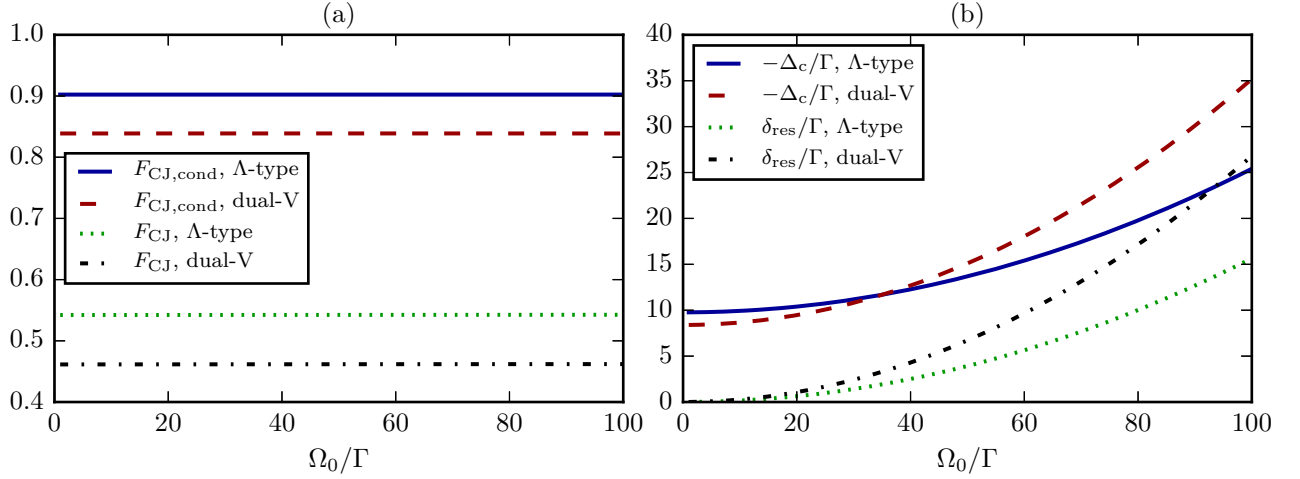


FIG. S12. (a) Unconditional and conditional Choi-Jamiolkowski fidelities for the Λ -type and dual-V schemes plotted as functions of the Rabi frequency of the classical drive Ω_0 for a fixed number of atoms $N = 10^4$ and $\Gamma_{1D}/\Gamma = 0.05$. Under EIT (storage and retrieval), $\Omega(z) = \Omega_0$. Under stationary light (scattering), $\Omega(z) = \Omega_0 \cos(k_0 z)$ and $\Omega_{\pm}(z) = \Omega_0 e^{\pm i k_0 z}$ for Λ -type and dual-V, respectively. The fidelities are plotted only for $t_b = 1$. For $t_b < 1$, they are likewise constant for the shown values of Ω_0/Γ . The bandwidth of the scattered photon B is ignored in the calculations, and we take the Sagnac interferometer to be perfectly aligned ($k_0 l_1 = k_0 l_2 = 0$). For storage and retrieval, we use the discretized continuum storage and retrieval kernels discussed in Sec. 6.4. (b) Plot of the optimal Δ_c and δ_{res} for the setups of (a).

We use Eq. (S173) to optimize over $\tilde{\sigma}$. The optimal $\tilde{\sigma}$ is obtained when

$$\frac{\pi^3(\Gamma_{1D} + \Gamma')}{2\Gamma_{1D}\sqrt{N}}\tilde{\sigma}^2 = \frac{1}{2} \frac{\Gamma'}{N\Gamma_{1D}} \frac{1}{\tilde{\sigma}^2}. \quad (\text{S174})$$

From this condition we get

$$\tilde{\sigma}^2 = \frac{1}{\pi^{3/2}N^{1/4}} \sqrt{\frac{\Gamma'}{\Gamma_{1D} + \Gamma'}} \quad (\text{S175})$$

and with this value of $\tilde{\sigma}$, Eq. (S173) becomes

$$F_{\text{CJ}} \approx 1 - \epsilon_b - \frac{\pi\Gamma'}{\Gamma_{1D}\sqrt{N}} - \frac{\pi^{3/2}\sqrt{\Gamma_{1D} + \Gamma'}\sqrt{\Gamma'}}{\Gamma_{1D}N^{3/4}} + \left(-\frac{1}{2} + \frac{3}{8}\epsilon_b + \frac{5\Gamma'\pi}{8\Gamma_{1D}\sqrt{N}} + \frac{\pi^{3/2}(7\Gamma_{1D} + 5\Gamma')}{16\Gamma_{1D}N^{3/4}} \sqrt{\frac{\Gamma'}{\Gamma_{1D} + \Gamma'}} \right) (k_0 l_1)^2. \quad (\text{S176})$$

To obtain Eqs. (7) and (9) of the main article, we set $\epsilon_b = 0$ and $\epsilon_b = 1 - R_0 = (\Gamma_{1D}\Gamma'N)/(8\Delta_c^2) = (\pi\Gamma')/(\Gamma_{1D}\sqrt{N})$, respectively. We see that for $N \rightarrow \infty$, the terms proportional to $N^{-3/4}$ approach zero faster than the terms proportional to $N^{-1/2}$. Hence, we have omitted the former terms in the main article. Furthermore, the $k_0 l_1$ dependent terms are also omitted, since we discuss them separately at the end of the main article. For parameters where the gate has a good performance, the parenthesis multiplying $(k_0 l_1)^2$ in Eq. (S176) is dominated by the constant term $-1/2$. In the main article, the total error $\sim (k_0 l)^2$ was quoted, where we have omitted the technical detail about two different fluctuating lengths (l_1 and l_2) and used l to refer to both of them.

Next, we calculate the conditional fidelity $F_{\text{CJ,cond}}$. Here, we neglect the Ω_0 dependent terms in Eqs. (S67), (S68), (S80) and (S81), since we expect them to cancel in the same way as for the unconditional fidelity according to the numerical calculations in Fig. S12. The imperfection of the Sagnac interferometer alignment is also neglected, since the error terms are expected to be roughly the same as for the unconditional fidelity according to the numerical calculations in Fig. S11. Since the conditional fidelity is given by $F_{\text{CJ,cond}} = F_{\text{CJ}}/P_{\text{suc}}$, the expansion of the ratio will contain higher order error terms than the expansion of the unconditional fidelity F_{CJ} . Hence, we need an expansion of F_{CJ} with more terms than in Eq. (S170). Including the second order terms and dividing out η_{EIT} (since it gets

canceled in $F_{\text{CJ,cond}}$), we get

$$\begin{aligned} \frac{F_{\text{CJ}}}{\eta_{\text{EIT}}} &\approx 1 - \epsilon_b - \frac{\Gamma_{1\text{D}}\Gamma'N}{16\Delta_c^2} - \frac{4\pi^2\Delta_c^2\Gamma'}{\Gamma_{1\text{D}}^3N^2} - \frac{4\pi^4\Delta_c^2(\Gamma_{1\text{D}} + \Gamma')}{\Gamma_{1\text{D}}^3N^2}\tilde{\sigma}^2 \\ &+ \left(\frac{1}{2}\epsilon_b + \frac{\Gamma_{1\text{D}}\Gamma'N}{32\Delta_c^2} + \frac{2\pi^2\Delta_c^2\Gamma'}{\Gamma_{1\text{D}}^3N^2} + \frac{2\pi^4\Delta_c^2(\Gamma_{1\text{D}} + \Gamma')}{\Gamma_{1\text{D}}^3N^2}\tilde{\sigma}^2 \right)^2 \end{aligned} \quad (\text{S177})$$

Using Eq. (6), we also get the success probability

$$\frac{P_{\text{suc}}}{\eta_{\text{EIT}}} = \frac{1}{4} \left(2(1 - \epsilon_b)^2 + \left(1 - \frac{\Gamma_{1\text{D}}\Gamma'N}{8\Delta_c^2} \right)^2 + R_{1,2} \right), \quad (\text{S178})$$

where

$$\begin{aligned} R_{1,2} &\approx \int |R_{1,s}(\tilde{z})|^2 |S(\tilde{z})|^2 d\tilde{z} \\ &= 1 - \frac{16\pi^2\Delta_c^2\Gamma'}{\Gamma_{1\text{D}}^3N^2} - \frac{16\pi^4\Delta_c^2(\Gamma_{1\text{D}} + \Gamma')}{\Gamma_{1\text{D}}^3N^2}\tilde{\sigma}^2 + \left(\frac{8\pi^2\Delta_c^2\Gamma'}{\Gamma_{1\text{D}}^3N^2} \right)^2 + \left(\frac{8\pi^4\Delta_c^2(\Gamma_{1\text{D}} + \Gamma')}{\Gamma_{1\text{D}}^3N^2} \right) (3\tilde{\sigma}^4) \\ &+ 2 \left(\frac{8\pi^2\Delta_c^2\Gamma'}{\Gamma_{1\text{D}}^3N^2} \right) \left(\frac{8\pi^4\Delta_c^2(\Gamma_{1\text{D}} + \Gamma')}{\Gamma_{1\text{D}}^3N^2} \right) \tilde{\sigma}^2. \end{aligned} \quad (\text{S179})$$

Using the above expressions, the conditional fidelity can be written

$$F_{\text{CJ,cond}} \approx 1 - \epsilon_{\text{cond},1} - \epsilon_{\text{cond},2}, \quad (\text{S180})$$

where

$$\epsilon_{\text{cond},1} = \frac{1}{4} \left(2\epsilon_b^2 + \left(\frac{\Gamma_{1\text{D}}\Gamma'N}{8\Delta_c^2} \right)^2 + \left(\frac{8\pi^2\Delta_c^2\Gamma'}{\Gamma_{1\text{D}}^3N^2} \right)^2 \right) - \frac{1}{16} \left(2\epsilon_b + \frac{\Gamma_{1\text{D}}\Gamma'N}{8\Delta_c^2} + \frac{8\pi^2\Delta_c^2\Gamma'}{\Gamma_{1\text{D}}^3N^2} \right)^2, \quad (\text{S181})$$

$$\epsilon_{\text{cond},2} = \frac{44\pi^8\Delta_c^4(\Gamma_{1\text{D}} + \Gamma')^2}{\Gamma_{1\text{D}}^6N^4}\tilde{\sigma}^4. \quad (\text{S182})$$

Using the Δ_c from Eq. (S172), we get

$$\epsilon_{\text{cond},1} = \frac{1}{2} \left(\epsilon_b^2 + \left(\frac{\pi\Gamma'}{\Gamma_{1\text{D}}\sqrt{N}} \right)^2 \right) - \frac{1}{4} \left(\epsilon_b + \frac{\pi\Gamma'}{\Gamma_{1\text{D}}\sqrt{N}} \right)^2, \quad (\text{S183})$$

$$\epsilon_{\text{cond},2} = \frac{11\pi^6(\Gamma_{1\text{D}} + \Gamma')^2}{\Gamma_{1\text{D}}^2N}\tilde{\sigma}^4. \quad (\text{S184})$$

If we choose $\epsilon_b = 0$, $\epsilon_{\text{cond},1}$ is the dominant error term with the value

$$\epsilon_{\text{cond},1} = \frac{1}{4} \left(\frac{\pi\Gamma'}{\Gamma_{1\text{D}}\sqrt{N}} \right)^2, \quad (\text{S185})$$

and $\epsilon_{\text{cond},2}$ can be neglected. If we choose $\epsilon_b = (\pi\Gamma')/(\Gamma_{1\text{D}}\sqrt{N})$, we get $\epsilon_{\text{cond},1} = 0$, and we need to keep $\epsilon_{\text{cond},2}$. The value of $\epsilon_{\text{cond},2}$ depends on the width $\tilde{\sigma}$ of the stored Gaussian spin wave. For simplicity, we use the value of $\tilde{\sigma}$ given by Eq. (S175), which makes the unconditional fidelity maximal. With this choice, the conditional fidelity is given by Eq. (10) of the main article. A comparison of the analytical formulas and the numerical results for F_{CJ} and $F_{\text{CJ,cond}}$ is shown in Fig. S13.

Next, we derive the correction to the unconditional fidelity due to non-zero bandwidth of the scattered photon B . The general expression for the fidelity is given by Eq. (S29). As discussed in the main article, we ignore the non-zero

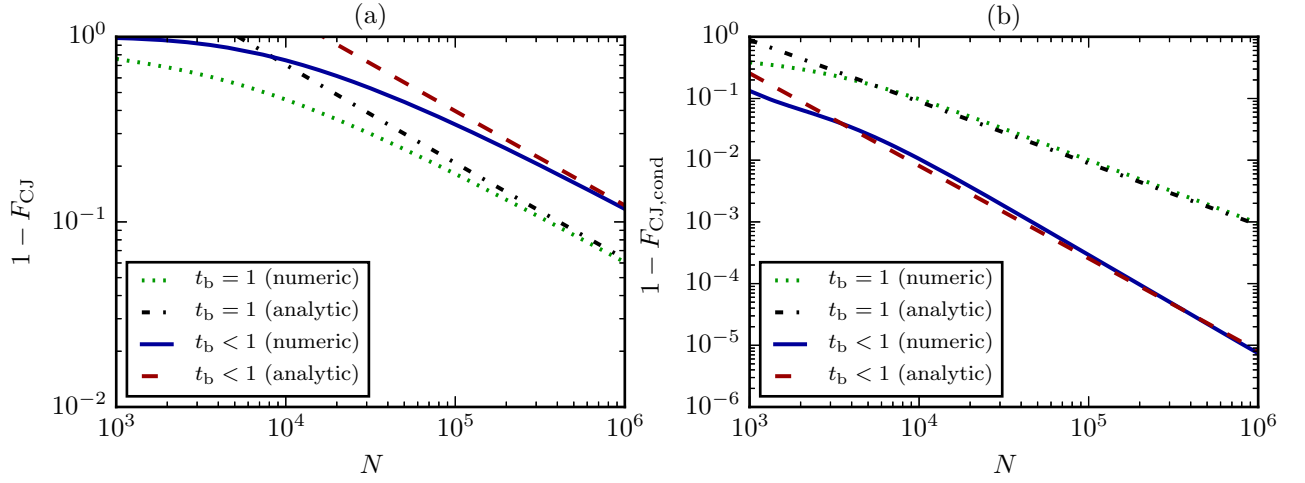


FIG. S13. Comparison of (a) unconditional and (b) conditional Choi-Jamiolkowski fidelities for the Λ -type scheme plotted as functions of the number of atoms N with fixed $\Gamma_{1D}/\Gamma = 0.05$ and $\Omega_0/\Gamma = 1$. Under EIT (storage and retrieval), $\Omega(z) = \Omega_0$. Under stationary light (scattering), $\Omega(z) = \Omega_0 \cos(k_0 z)$. Dotted green curves are the numerically calculated fidelities with $t_b = 1$. Dash-dotted black curves are the approximate analytical results given by Eq. (7) (unconditional) and Eq. (8) (conditional) of the main article. Solid blue curves are the numerically calculated fidelities with t_b chosen such that the entanglement swap fidelity (which is approximately equal to the conditional Choi-Jamiolkowski fidelity as shown in Fig. S6) is maximal. The dashed red curves are the approximate analytical results given by Eq. (9) (unconditional) and Eq. (10) (conditional) of the main article. For storage and retrieval in the numerical calculations, we use the discretized continuum storage and retrieval kernels discussed in Sec. 6.4.

bandwidth in the last term since the variation of r_1 and t_1 with frequency around the resonance detuning δ_{res} is smaller than variation of r_0 and t_0 . Hence, we approximate

$$\frac{1}{\eta_{\text{EIT}}} \iint \phi_{A,\text{out},0}^*(t_A) \phi_{A,\text{out},1}(t_A, \delta_B) |\phi_B(\delta_B)|^2 dt_A d\delta_B \approx (1/\eta_{\text{EIT}}) \int \phi_{A,\text{out},0}^*(t) \phi_{A,\text{out},1}(t) dt = R_{1,1} \quad (\text{S186})$$

such that the expression for the fidelity becomes

$$F_{\text{CJ}} = \frac{\eta_{\text{EIT}}}{16} \left| 2t_b + \int R_0(\delta_B) |\phi_B(\delta_B)|^2 d\delta_B - R_{1,1} \right|^2. \quad (\text{S187})$$

Using Eqs. (S69) and (S70) together with the expressions $t_0 \approx 1 - r_0$ and $R_0 = -(r_0 - t_0)$ and defining the spectral width of photon B by $\sigma_B^2 = \int (\delta - \delta_{\text{res}})^2 |\phi_B(\delta_B)|^2 d\delta_B$, we get (using $k_{0l_1} = k_{0l_2} = 0$ for brevity)

$$\int R_0(\delta) |\phi_B(\delta_B)|^2 d\delta_B \approx R_0(\delta_{\text{res}}) - (4/w^2) \sigma_B^2 \approx 1 - \frac{\Gamma_{1D} \Gamma' N}{8\Delta_c^2} - \frac{\pi^2 \Gamma' |\Omega_0|^2}{\Delta_c^2 \Gamma_{1D} N} - \frac{\Gamma_{1D}^6 N^6}{512 \Delta_c^4 |\Omega_0|^4 \pi^4} \sigma_B^2. \quad (\text{S188})$$

Using the optimal Δ_c from Eq. (S172), this becomes

$$\int R_0(\delta) |\phi_B(\delta_B)|^2 d\delta_B \approx 1 - \frac{\pi \Gamma'}{\Gamma_{1D} \sqrt{N}} - \frac{8\pi^3 \Gamma' |\Omega_0|^2}{\Gamma_{1D}^3 N^{5/2}} - \frac{\Gamma_{1D}^2 N^3}{8 |\Omega_0|^4 \pi^2} \sigma_B^2. \quad (\text{S189})$$

Using the same optimal Δ_c , Eq. (S169) becomes

$$R_{1,1} \approx \int R_{1,s}(\tilde{z}) |S(\tilde{z})|^2 d\tilde{z} = - \left(1 - \frac{\pi \Gamma'}{\Gamma_{1D} \sqrt{N}} + \frac{8\pi^3 \Gamma' |\Omega_0|^2}{\Gamma_{1D}^3 N^{5/2}} - \frac{\pi^3 (\Gamma_{1D} + \Gamma')}{\Gamma_{1D} \sqrt{N}} \tilde{\sigma}^2 \right) \quad (\text{S190})$$

We see that the terms in Eqs. (S189) and (S190) that are proportional to $|\Omega_0|^2$ cancel upon insertion into Eq. (S187) (as already noted above for the case with $\sigma_B = 0$). With the optimal value of $\tilde{\sigma}$ (S175), we get

$$F_{\text{CJ}} \approx 1 - \epsilon_b - \frac{\pi \Gamma'}{\Gamma_{1D} \sqrt{N}} - \frac{\pi^{3/2} \sqrt{\Gamma_{1D} + \Gamma'} \sqrt{\Gamma'}}{\Gamma_{1D} N^{3/4}} - \frac{\Gamma_{1D}^2 N^3}{16 |\Omega_0|^4 \pi^2} \sigma_B^2. \quad (\text{S191})$$

Compared to Eq. (S176), there is an extra error term that depends on σ_B (and the $k_0 l_1$ dependent term is omitted).

To find the allowed value of σ_B , we require the error in Eq. (S176) due to non-zero σ_B to be equal to the biggest σ_B independent one, i.e.

$$\frac{\pi\Gamma'}{\Gamma_{1D}\sqrt{N}} = \frac{\Gamma_{1D}^2 N^3}{16|\Omega_0|^4 \pi^2} \sigma_B^2. \quad (\text{S192})$$

This gives

$$\frac{1}{\sigma_B} = \frac{\Gamma_{1D}^{3/2} N^{7/4}}{4\pi^{3/2} \sqrt{\Gamma'} |\Omega_0|^2}. \quad (\text{S193})$$

This is the expression used to determine the scattering time in the main article.

10. DEPENDENCE ON POSITIONS OF THE ATOMS

While the Λ -type scheme is highly sensitive to the exact placement of the atoms, the dual-V scheme is much less sensitive. To verify this, we numerically evaluate the gate performance for various placements of the atoms. First, we investigate the dependence for regularly placed dual-V atoms with different interatomic spacings d . In Fig. S14, we see that for $k_0 d$ different from multiples of $\pi/2$, both the conditional and unconditional fidelities are approximately constant.

Second, we consider randomly placed dual-V atoms. In Fig. S15, the fidelities with regular and random placement are seen to have almost the same behavior. For larger values of Γ_{1D}/Γ , the agreement between the two different placements becomes less good. They still have qualitatively the same behavior, but the random placement has slightly worse performance.

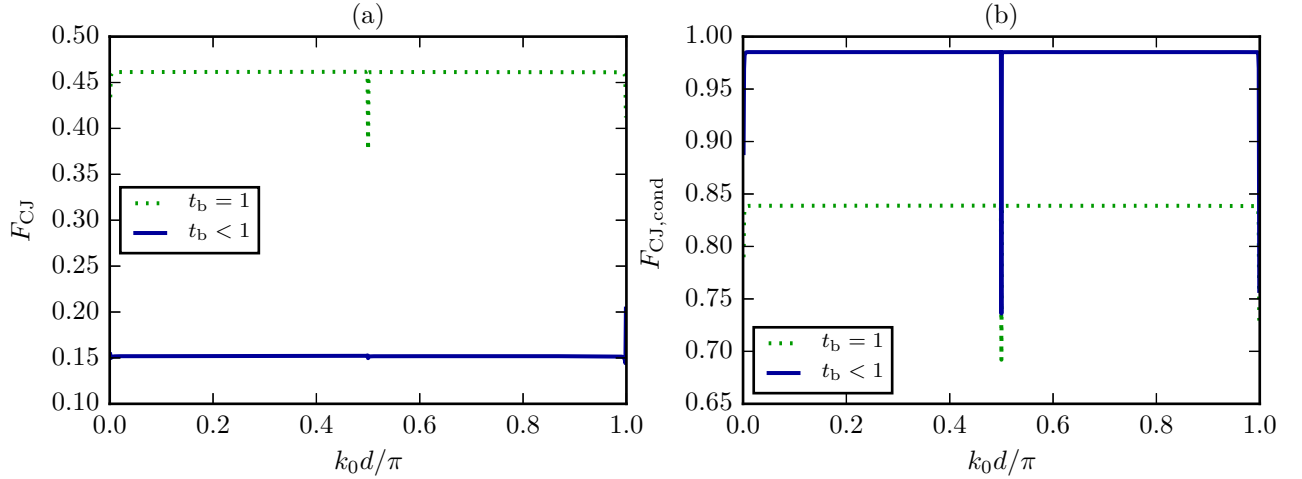


FIG. S14. (a) Unconditional and (b) conditional Choi-Jamiolkowski fidelities for the dual-V scheme plotted as functions of the interatomic spacing d times the photon wave vector k_0 for fixed number of atoms $N = 10^4$, $\Gamma_{1D}/\Gamma = 0.05$, and $\Omega_0/\Gamma = 1$. Under EIT (storage and retrieval), $\Omega(z) = \Omega_0$. Under stationary light (scattering), $\Omega_{\pm}(z) = \Omega_0 e^{\pm i k_0 z}$. For storage and retrieval, we use the discretized continuum storage and retrieval kernels discussed in Sec. 6.4.

-
- [S1] L.-M. Duan, M. D. Lukin, J. I. Cirac, and P. Zoller, *Nature* **414**, 413 (2001).
[S2] N. Sangouard, C. Simon, H. de Riedmatten, and N. Gisin, *Rev. Mod. Phys.* **83**, 33 (2011).
[S3] N. Sangouard, C. Simon, B. Zhao, Y.-A. Chen, H. de Riedmatten, J.-W. Pan, and N. Gisin, *Phys. Rev. A* **77**, 062301 (2008).
[S4] J. Borregaard, P. Kómár, E. M. Kessler, M. D. Lukin, and A. S. Sørensen, *Phys. Rev. A* **92**, 012307 (2015).

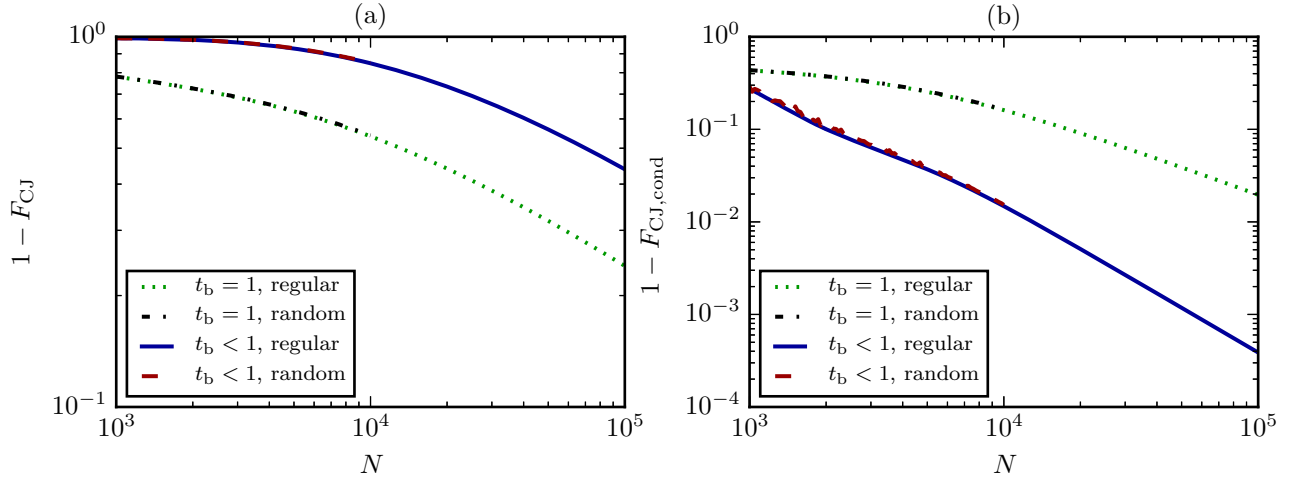


FIG. S15. Comparison of (a) unconditional and (b) conditional Choi-Jamiolkowski fidelities for the dual-V scheme with different placement of the atoms (regular or random) plotted as functions of the number of atoms N with fixed $\Gamma_{1D}/\Gamma = 0.05$ and $\Omega_0/\Gamma = 1$. Under EIT (storage and retrieval), $\Omega(z) = \Omega_0$. Under stationary light (scattering), $\Omega_{\pm}(z) = \Omega_0 e^{\pm i k_0 z}$. The regularly placed atoms have positions $z_j = jd$ for $d = 0.266\pi/k_0$ and $0 \leq j \leq N-1$. The positions of the randomly placed atoms are chosen from the uniform distribution over the whole ensemble and then sorted in increasing order. For random placement, we average over 100 ensemble realizations. For storage and retrieval, we use the discretized continuum storage and retrieval kernels discussed in Sec. 6.4.

- [S5] S. Das, A. Grankin, I. Iakoupov, E. Brion, J. Borregaard, R. Boddeda, I. Usmani, A. Ourjoumtsev, P. Grangier, and A. S. Sørensen, *Phys. Rev. A* **93**, 040303 (2016).
- [S6] D. A. Steck, “Rubidium 87 D Line Data,” Available online at <http://steck.us/alkalidata> (revision 2.1.5, 13 January 2015).
- [S7] P. Walther, M. D. Eisaman, A. André, F. Massou, M. Fleischhauer, A. S. Zibrov, and M. D. Lukin, *International Journal of Quantum Information* **05**, 51 (2007).
- [S8] I. Vurgaftman and M. Bashkansky, *Phys. Rev. A* **87**, 063836 (2013).
- [S9] S. A. Moiseev and B. S. Ham, *Phys. Rev. A* **73**, 033812 (2006).
- [S10] F. E. Zimmer, J. Otterbach, R. G. Unanyan, B. W. Shore, and M. Fleischhauer, *Phys. Rev. A* **77**, 063823 (2008).
- [S11] I. Iakoupov, J. R. Ott, D. E. Chang, and A. S. Sørensen, *Phys. Rev. A* **94**, 053824 (2016).
- [S12] I. Iakoupov, *Enhancement of optical nonlinearities with stationary light*, Ph.D. thesis, University of Copenhagen (2016).
- [S13] I. Iakoupov and A. S. Sørensen, In preparation.
- [S14] A. Gilchrist, N. K. Langford, and M. A. Nielsen, *Phys. Rev. A* **71**, 062310 (2005).
- [S15] I. H. Deutsch, R. J. C. Spreeuw, S. L. Rolston, and W. D. Phillips, *Phys. Rev. A* **52**, 1394 (1995).
- [S16] T. Peters, Y.-H. Chen, J.-S. Wang, Y.-W. Lin, and I. A. Yu, *Opt. Lett.* **35**, 151 (2010).
- [S17] G. Bertocchi, O. Alibart, D. B. Ostrowsky, S. Tanzilli, and P. Baldi, *Journal of Physics B: Atomic, Molecular and Optical Physics* **39**, 1011 (2006).
- [S18] M. Bradford, K. C. Obi, and J.-T. Shen, *Phys. Rev. Lett.* **108**, 103902 (2012).
- [S19] D. E. Chang, A. H. Safavi-Naeini, M. Hafezi, and O. Painter, *New Journal of Physics* **13**, 023003 (2011).
- [S20] T. Caneva, M. T. Manzoni, T. Shi, J. S. Douglas, J. I. Cirac, and D. E. Chang, *New Journal of Physics* **17**, 113001 (2015).
- [S21] A. V. Gorshkov, A. André, M. D. Lukin, and A. S. Sørensen, *Phys. Rev. A* **76**, 033805 (2007).
- [S22] F. Reiter and A. S. Sørensen, *Phys. Rev. A* **85**, 032111 (2012).